FUEL-OPTIMAL REORIENTATION OF A SPINNING BODY

By

Robert T. Wingate

Thesis submitted to the Graduate Faculty of the

Virginia Polytechnic Institute

in candidacy for the degree of

DOCTOR OF PHILOSOPHY

in

Engineering Mechanics

July 1970

(NASA-CR-176696:NAS 1.26:176696) N86-71440
FUEL-OPTIMAL REORIENTATION OF A SPINNING BODY Ph.D. Thesis (Virginia Polytechnic Inst., Blacksburg.) 133 p Unclas
00/34 00690

FUEL-OPTIMAL REORIENTATION OF A SPINNING BODY

By

Robert T. Wingate

ABSTRACT

The reorientation of a spin-stabilized body is inherently resisted by gyroscopic moments and can require significant control effort. For a conventional reaction-jet control system this may result in prohibitive fuel requirements.

The objective of this paper is to investigate the fuel-optimal control problem of reorienting a symmetrical spinning body within a prescribed time by means of a single body-fixed jet. A canonical set of linearized, dimensionless state equations is derived for an idealized representation of a spinning body. Pontryagin's minimum principle is then used to derive the optimal control equations in the form of a two-point boundary value problem. The optimal control law is shown to be of the "bang-bang" type.

A numerical algorithm is presented for solution of the two-point boundary value problem. Numerical solutions obtained from a computer program incorporating the algorithm are then presented for several typical sets of conditions. These results are used as a basis for the development of an approximation to the optimal control. Many of the fundamental properties of the fuel-optimal control of spinning bodies are established and a technology base is provided for extension to more complex situations.

FUEL-OPTIMAL REORIENTATION OF A SPINNING BODY

by

Robert T. Wingate

Thesis submitted to the Graduate Faculty of the

Virginia Polytechnic Institute

in partial fulfillment for the degree of

DOCTOR OF PHILOSOPHY

in

Engineering Mechanics

APPROVED:

J. Counts

Chairman, Dr. J. Counts

R. Thomas Davis

Dr. R. T. Davis

G. W. Swift

Dr. G. W. Swift

B. E. Reed

Dr. B. E. Reed

Frederick Lutze

Dr. F. H. Lutze

July 1970

Blacksburg, Virginia

II. ACKNOWLEDGMENTS

The author wishes to thank the NASA for its support of this study and Mrs. Edna Davidson, Mrs. Yvonne Powell, and Mrs. Norma Price for their expedience in typing the manuscript for reproduction. In particular the author wishes to express his appreciation to Mrs. Maria V. Stephens for her help in the programing of the computational algorithm.

III. TABLE OF CONTENTS

CHAPTER		PAGE
I.	TITLE	i
II.	ACKNOWLEDGMENTS	ii
III.	TABLE OF CONTENTS	iii
IV.	LIST OF TABLES AND FIGURES	vi
V.	INTRODUCTION	1
VI.	SYMBOLS	5
VII.	SYSTEM EQUATIONS OF MOTION	8
	A. Mathematical Model	8
	B. Euler Equations of Motion	10
	C. Linearized Equations of Motion	12
	D. Nondimensional Equations	14
	E. State Space Formulation	16
	F. Canonical Transformation	17
VIII.	FUEL-OPTIMAL CONTROL	21
	A. Statement of the Problem	21
	B. Necessary Conditions for Optimality	22
	1. Minimum Principle	22
	2. Optimal Control Equations	24
	C. Controllability	26
	D. Singular Control	28
	E. Uniqueness of Optimal Control	33
	F. Lower Bounds on Minimum Fuel	36

CHAPTER PAGE

IX. SOLUTION OF THE BOUNDARY VALUE PROBLEM 38

A. Augmented Performance Index 39

B. Computational Algorithm 44

1. Iterative Gradient Search 45

2. Optimal Step Search 48

3. Fletcher-Powell Digital Computer Subroutine. . 53

C. Numerical Determination of the Augmented Performance Function and Its Gradient 53

1. Determination of Switching Times 54

2. Integration of the System Equation 58

D. Digital Computer Program 60

X. THE EFFECTS OF SYSTEM PARAMETERS ON THE OPTIMAL CONTROL 63

A. Impulsive Fuel-Optimal Controls 63

1. Two-Impulse Fuel-Optimal Control 64

2. Approximations to Impulsive Controls 66

B. Typical Solutions for Various Classes of Initial Conditions 68

C. The Effects of the System Parameters on Minimum Fuel Consumption 89

XI. APPROXIMATE FEEDBACK OPTIMAL CONTROL 97

A. Simplification of Switching Function 98

B. Switching Function Phase Angles 98

CHAPTER PAGE

C. Switching Function Amplitudes 102

D. Feedback Control Logic 105

XII. CONCLUSIONS 108

XIII. APPENDICES 111

A. Modified Jordan Transformation Matrix 111

1. Jordan Canonical Form 111

2. Modified Jordan Canonical Form 112

B. Physical Significance of Canonical variables . . . 114

1. Canonical State Variables 114

2. Canonical Control Variables 120

XIV. REFERENCES 121

XV. VITA 123

IV. LIST OF TABLES AND FIGURES

TABLE PAGE

10.1 Impulsive efficiency as a function of the firing sector half-angle 69

10.2 Dimensionless input parameter values for typical solutions 71

10.3 Computed parameter values for typical solutions 71

FIGURE

7.1 Typical mathematical models for a single jet control actuator 9

7.2 Euler angle orientation of body axes with respect to inertial axes (the order of rotation is ψ, θ, φ) 11

8.1 Switching function behavior 32

9.1 Extrapolation search 51

9.2 Behavior of cubic fit 51

9.3 Type "A" crossings ($f_{s_2}/f_{s_1} < 0$) 55

9.4 Type "B" crossings ($f_{s_1}/f_{s_2} < 0$) and $f_{s_1}\dot{f}_{s_1} < 0$) . . . 55

9.5 False type "B" crossings ($\dot{f}_{s_1}/\dot{f}_{s_2} < 0$ and $f_{s_1}\dot{f}_{s_1} < 0$) 57

9.6 Slope change configurations ($\dot{f}_{s_1}/\dot{f}_{s_2} < 0$) 57

9.7 Flow diagram for digital computer program 61

10.1 Trajectory in the ψ-θ plane resulting from impulsive control 65

FIGURE PAGE

10.2 Class 1 fuel-optimal two-impulse control 65

10.3 Class 2 fuel-optimal two-impulse control 67

10.4 Cosine loss of rotating reaction jet 67

10.5 Solutions for class 1 initial conditions (case 1, r = 0.1) 72

10.6 Solutions for class 2 initial conditions (case 2, r = 0.1) 74

10.7 Solutions for class 3 initial conditions (case 3, r = 0.1) 76

10.8 Solutions for class 4 initial conditions (case 4, r = 0.1) 78

10.9 Solutions for class 1 initial conditions (case 5, r = 1.9) 80

10.10 Solutions for class 2 initial conditions (case 6, r = 1.9) 82

10.11 Solutions for class 3 initial conditions (case 7, r = 1.9) 84

10.12 Solutions for class 4 initial conditions (case 8, r = 1.9) 86

10.13 Typical momentum and nutation shift due to an impulse for class 1 initial conditions 93

10.14 Fuel consumption ratio as a function of the final time ratio 93

FIGURE		PAGE
11.1	Switching function lower envelope	99
11.2	Phase relationships in a typical ψ-θ trajectory . . .	99
11.3	Bi-level switching function	103
B.1	Angular momentum coordinates (ψ_h, θ_h)	115
B.2	Nutation coordinates (ψ_n, θ_n)	115
B.3	Torque-free nutational motion in ψ-θ plane	117
B.4	Deviation in angular momentum due to an impulsive torque	117

V. INTRODUCTION

The payloads of many high altitude research rockets are spin-stabilized and have a requirement to attain a given orientation relative to inertial space after reaching the upper atmosphere. Spinning space stations or satellites may also have similar reorientation requirements. Considerable effort has, therefore, been expended in the study and development of various attitude control systems for spinning bodies with particular emphasis on reaction control systems (e.g., refs. 1-8).

The hardware reliability and simplicity of reaction control systems make them attractive. However, a significant amount of control effort (or fuel) is required to overcome spin stability in a reorientation maneuver. The amount of time allowed for reorientation further affects the fuel consumption. As a result, fuel requirements can become the critical control system design factor in payloads with weight and space limitations. This is particularly true in space stations with long operational life. Control laws which minimize fuel consumption are consequently of considerable interest.

The objective of this paper is to investigate the fuel-optimal control problem of reorienting a symmetrical spinning body within a prescribed time by means of a single body-fixed jet. This investigation includes the development of a numerical algorithm to solve the open-loop optimal control problem; a study of the effect of system parameters on fuel consumption; and a study of logic which could be

applied to the design of a closed-loop system which approximates the optimal. The reorientation problem is inherently one of short-term control as opposed to the long-term orientation holding problem where a commanded attitude is held in the face of disturbing torques.

At the beginning of the control period, the spinning body is, in general, nutating (coning) about the angular momentum vector which is fixed in space and pointing in an undesired direction. The control logic must then simultaneously damp the nutation and turn the angular momentum vector to the desired orientation within a given time. Synthesis of the optimal control (i.e., the determination of the optimal feedback control law) is very difficult because of the order and complexity of the differential equations of motion. Some results have been obtained for the fuel-optimal nutation reduction problem (refs. 9, 10) and the time-optimal nutation reduction problem (refs. 11, 12). There has also been some progress made in the related time-optimal orientation problem (ref. 13). The present work, however, is the first known attempt to analyze the theoretical fuel-optimal control law for the combined task of nutation reduction and angular momentum reorientation.

The mathematical model used in the present analysis has been idealized in order to isolate the basic factors governing the optimal control from the real world complications such as small extraneous torques, friction, and time lags. The modified Euler equations for spin about an axis of symmetry are used to derive the equations of motion in terms of the classical Euler angles. These equations of

motion are nonlinear and highly coupled. They are, therefore, linearized, nondiminsionalized and transformed to the Jordan canonical form and the canonical variables are shown to correspond to the nutational and precessional motion. The resulting matrix state equation is then in the most advantageous form to formulate the optimal control problem.

The control problem consists, mathematically speaking, of a fourth-order system with fixed end points, a fixed final time, and inequality constraints on the control variable. Pontryagin's minimum principle is used to obtain the necessary conditions for optimality. The resulting optimal control is shown to be a "bang-bang" type which is dependent on a switching function containing four unknown constants. Determination of the optimal control problem is then reduced to the difficult solution of a two-point boundary value problem in which half of the boundary conditions are specified at the initial time and half at the final time. The solutions to problems of this nature can only be obtained numerically. Additional factors such as controllability, singular controls, and uniqueness are also investigated, and a limiting bound on the minimum fuel consumption is derived.

A new computational procedure is developed to solve the two-point boundary value problem in an efficient manner. This method combines a unique augmented performance index (which has a closed-form gradient expression) with an iterative gradient search and uses patched closed-form solutions to integrate the equations of motion. The method results

directly from the minimum principle and is applicable to any linear system. It is far superior to any of the presently used methods for solving bang-bang fuel-optimal control problems. All of the logic in the computational algorithm has been incorporated into a digital computer program which yields solutions for virtually any arbitrary conditions.

An investigation is made of the effects various system parameters have on the optimal control solutions and on the minimum fuel consumption. The combined effects of all of the system parameters are established by an empirical equation which indicates the minimum final time required for minimum fuel consumption. Finally, the results of the numerical solutions are utilized to derive an approximate feedback control which closely approximates optimal.

VI. SYMBOLS

A	square matrix in the canonical state equation (see eq. (7.22))
A_1, A_2	switching function amplitude constants (see eq. (8.25))
B	approximate switching function amplitude constant (see fig. 11.3)
b	vector in the canonical state equation (see eq. (7.23))
C	square matrix in the state equation (see eq. (7.17))
D	amplitude of switching function envelope (see eq. (8.31))
d	vector in the state equation (see eq. (7.18))
f_s	switching function (see eq. (8.12))
g	gradient vector (see eq. (9.33))
H	Hamiltonian function (see eq. (8.3))
h	angular momentum vector in the ψ-θ plane (see fig. B.3)
I	identity matrix
I_a	axial moment of inertial about the body x axis (see fig. 7.2-a), slug-ft^2
I_t	transverse moment of inertia about the body y or z axis (see fig. 7.2-a), slug-ft^2
J	performance index (see eq. (8.2))
$\bar{J}$	augmented performance index (see eq. (9.1))
M	applied control torque (see fig. 7.2-b), ft-lb
M_x, M_y, M_z	components of M along the x,y,z body axes, ft-lb
n	nutation vector in the ψ-θ plane (see fig. B.3); also, an integer

P	Jordan transformation matrix (see eq. (A.1))
$\bar{P}$	Modified Jordan transformation matrix (see eq. (A.9))
p	costate (or adjoint) vector, dimensionless
p_i	elements of the costate vector, $i = 1$ through 4
r	inertia ratio, I_a/I_t
T	nondimensional final time
t	nondimensional time
U	subset of the Euclidian space R_1, $\{u: \ 0 \leq u \leq u_{max}\}$
u	canonical control variable, $M/I_a\Omega^2$, dimensionless
x	canonical state vector, dimensionless
x_i	elements of the canonical state vector, $i = 1$ through 4
α	total angular displacement vector in the ψ-θ plane, (see fig. B.3)
β_1, β_2	switching function phase angles (see eq. (8.25))
δ	switching function phase angle, function of time, (see eq. (8.32))
δ_1, δ_2	argument of the initial angular momentum, nutation vector in the ψ-θ plane (see fig. 11.2)
ζ	argument of the nutation vector in the ψ-θ plane, a function of time
θ	Euler angle describing pitch motion (see fig. 7.2-a)
κ	angular bounds on the nutation circle firing arc (see fig. 10.13)
λ	switching function amplitude ratio, A_2/A_1-1

μ	magnitude of nondimensional impulsive control torque (see eq. (10.1))
ν	nondimensional control torque, $M/I_t\Omega^2$, (see eq. (7.11))
σ	ratio of the magnitude of the nutation vector to the magnitude of the angular momentum vector, $\|n\|/\|h\|$
τ	time, sec
φ	Euler angle describing roll motion (see fig. 7.2-a)
ψ	Euler angle describing yaw motion (see fig. 7.2-a)
Ω	spin rate, a constant, rad/sec
$\omega_x,\omega_y,\omega_z$	angular velocity components of the nonspinning coordinate axes, rad/sec

Superscripts

*	corresponds to the optimal value
'	transpose of a matrix
·	a dot over the quantity denotes the derivative with respect to nondimensional time, t

VII. SYSTEM EQUATIONS OF MOTION

Before the optimal control problem can be formulated, it is necessary to obtain the governing set of differential equations which describe the state of the proposed dynamical system as a function of time. In this chapter we derive the governing differential equation for an assumed mathematical model. Through a series of simplifying transformation, these equations are then reduced to a desired format for solution of the optimal control problem.

A. Mathematical Model

Typical mathematical models for the subject analysis are shown on figure 7.1. The vehicle is considered to be symmetric about its spin axis. Both attitude and rate control are achieved by a single-body fixed-reaction jet which produces a torque about the center of mass and causes a gyroscopic precession of the spin axis. The desired control is attained by varying the roll orientation and duration of the thrust.

It is assumed that the mass of the control fuel is small in comparison to the overall mass of the vehicle and, thus, the mass and inertia properties of the system remain constant as control fuel is expended. Further, it is assumed that the jet turns off and on instantly upon command. That is, the effects of such things as valve hysteresis, friction, and time lag are considered negligible. The vehicle is assumed to be operating in an environment such that the torques due to aerodynamics, gravity gradient, solar radiation pressure,

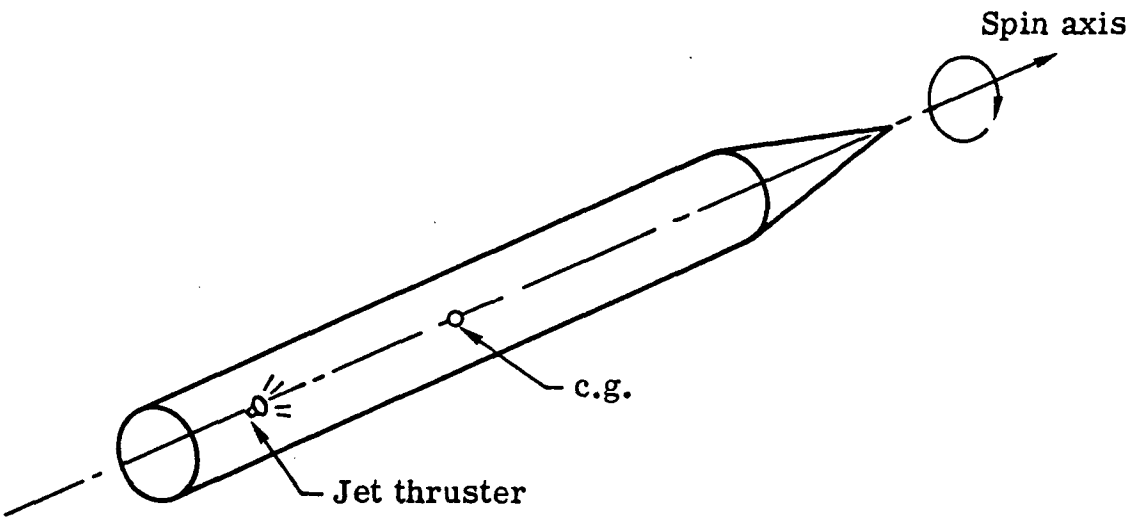

(a) Rod shaped body ($I_a / I_t < 1$)

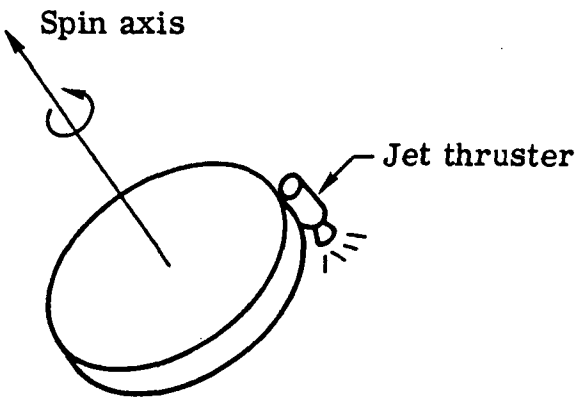

(b) Disc shaped body ($I_a / I_t > 1$)

Figure 7.1.- Typical mathematical models for a single jet control actuator.

etc., produce only long-term effects and can be neglected for the subject short-term control problem.

B. Euler Equations of Motion

The reference coordinate systems and the Eulerian angles used to describe the system motions are shown on figure 7.2-a. The equations of motion of the vehicle in the nonspinning x,y,z coordinate system are given by the modified Euler equations of reference 14 as

$$I_a\left(\frac{d\omega_x}{d\tau} + \frac{d^2\varphi}{d\tau^2}\right) = M_x,$$

$$I_t \frac{d\omega_y}{d\tau} - (I_t - I_a)\omega_z\omega_x + I_a \frac{d\varphi}{d\tau}\omega_z = M_y, \qquad (7.1)$$

and

$$I_t \frac{d\omega_z}{d\tau} + (I_t - I_a)\omega_x\omega_y - I_a \frac{d\varphi}{d\tau}\omega_y = M_z$$

where τ denotes times ω_x, ω_y, and ω_z are the components of the angular velocity of the nonspinning coordinate axes; M_x, M_y, and M_z are the external moments about the x,y,z axes; $\frac{d\varphi}{d\tau}$ is the spin rate of the vehicle about the x axis; I_a is the axial moment of inertia about the x axis; and I_t is the transverse moment of inertia about the y and z axes. Referring to figure 7.2-a and summing the orthogonal projections of $\frac{d\psi}{d\tau}$ and $\frac{d\theta}{d\tau}$ onto each of the axes in the x,y,z system, we find that

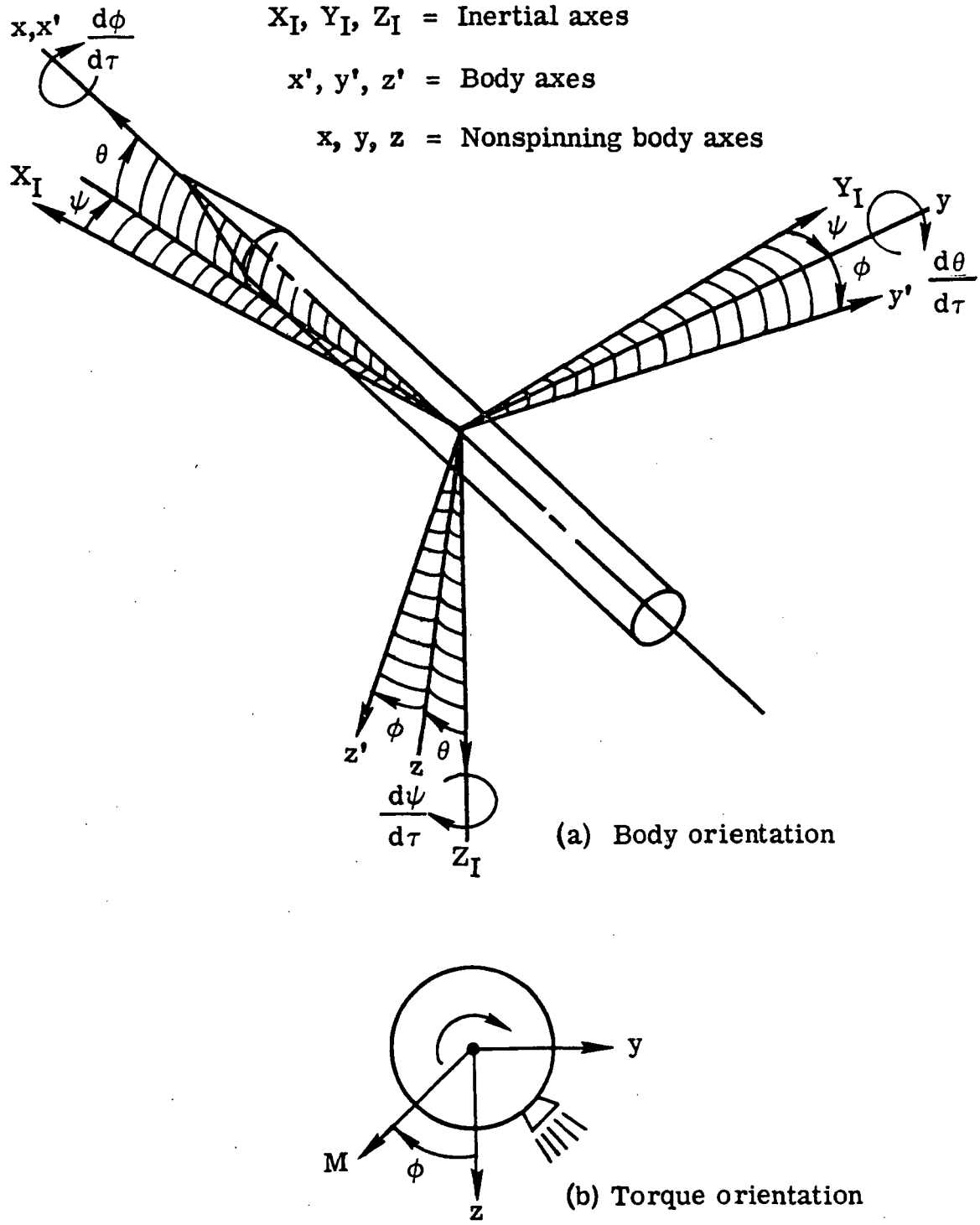

Figure 7.2.- Euler angle orientation of body axes with respect to inertial axes (the order of rotation is ψ, θ, Φ).

$$\omega_x = -\frac{d\psi}{d\tau} \sin\theta,$$

$$\omega_y = \frac{d\theta}{d\tau}, \tag{7.2}$$

and

$$\omega_z = \frac{d\psi}{d\tau} \cos\theta .$$

Also, from figure 7.2-b the orthogonal projection of the applied torque (M) onto the x,y,z axes gives

$$M_x = 0,$$

$$M_y = -M \sin\varphi,$$

and (7.3)

$$M_z = M \cos\varphi .$$

The complete angular motion of the system is then governed by a set of equations obtained from the substitution of equations (7.2) and (7.3) into equation (7.1).

C. Linearized Equations of Motion

It is seen that the foregoing set of differential equations are coupled and nonlinear. A better insight into the fundamentals of synthesizing the optimal control can be obtained by linearizing these equations and reducing them to a convenient form for solution.

If we assume that the angle θ and the angular rate $\frac{d\psi}{d\tau}$ are small then equations (7.2) can be approximated by

$$\omega_x \approx 0,$$

$$\omega_y \approx \frac{d\theta}{d\tau}, \tag{7.4}$$

and

$$\omega \approx \frac{d\psi}{d\tau}.$$

These linearizing assumptions imply that the angular momentum vector remains approximately in the yaw (ψ) plane and that the nutation of the spin axis about the angular momentum vector is small. These assumptions are not as restrictive as they first appeared since the angle ψ can be of any size, even 180°. Without loss of generality one can often choose the initial position of the coordinate systems such that the angular motion lies predominately in the yaw plane.

The substitution of equations (7.3) and (7.4) into equations (7.1) gives the linearized equations of motion in terms of the Eulerian angles as

$$I_a \frac{d^2\varphi}{d\tau^2} = 0,$$

$$I_t \frac{d^2\theta}{d\tau^2} + I_a \frac{d\varphi}{d\tau}\frac{d\psi}{d\tau} = -M \sin \varphi, \tag{7.5}$$

and

$$I_t \frac{d^2\psi}{d\tau^2} - I_a \frac{d\varphi}{d\tau} \frac{d\theta}{d\tau} = M \cos \varphi \ .$$

Noting from the first of equations (7.5) that $\frac{d\varphi}{d\tau} = \Omega$ (a constant), the remaining equations of equations (7.5) can be written as

$$I_t \frac{d^2\theta}{d\tau^2} + I_a\Omega \frac{d\psi}{d\tau} = - M \sin \Omega\tau$$

and (7.6)

$$I_t \frac{d^2\psi}{d\tau^2} - I_a\Omega \frac{d\theta}{d\tau} = M \cos \Omega\tau,$$

since $\varphi(0) = 0$. Equations (7.6) are linear and completely describe the motion for θ and $\frac{d\psi}{d\tau}$ small.

D. Nondimensional Equations

In order to reduce the number of parameters governing the motion, it is convenient to reduce equations (7.6) to dimensionless form. If we introduce the nondimensional time

$$t = \Omega\tau \tag{7.7}$$

then

$$\frac{d}{d\tau} = \frac{d}{dt} \frac{dt}{d\tau} = \Omega \frac{d}{dt} \tag{7.8}$$

and

$$\frac{d^2}{d\tau^2} = \Omega \frac{d}{dt}\left(\Omega \frac{d}{dt}\right) = \Omega^2 \frac{d^2}{dt^2} . \tag{7.9}$$

The substitution of equations (7.7) through (7.9) into equations (7.6) leads to

$$\ddot{\theta} + r\dot{\psi} = - \nu \sin t \tag{7.10}$$

and

$$\ddot{\psi} - r\dot{\theta} = \nu \cos t \tag{7.11}$$

where

$$r = \frac{I_a}{I_t} , \tag{7.12}$$

$$\nu = \frac{M}{I_t \Omega^2} , \tag{7.13}$$

and the dots denote the derivative with respect to the nondimensional time t. The inertia ratio, r, always falls between 0 (for a slender rod) and 2 (for a thin disc).

E. State Space Formulation

Modern optimal control theory for linear systems has been developed predominately from the state-space representation of the system equations of motion. To transform equations (7.10) and (7.11), which govern the motion of the subject system, into this useful notation let us introduce the following auxiliary variables:

$$\begin{aligned} y_1 &= \psi, \\ y_2 &= \dot{\psi}, \\ y_3 &= \theta, \end{aligned} \tag{7.14}$$

and

$$\dot{y}_4 = \dot{\theta} .$$

Then, from equations (7.10), (7.11), and (7.14) the equations of motion of the system can be written as a set of first order equations in matrix-vector notation as

$$\dot{y}(t) = Cy(t) + \nu(t)\, d(t) \tag{7.15}$$

where

$$y = \begin{Bmatrix} y_1 \\ y_2 \\ y_3 \\ y_4 \end{Bmatrix}, \tag{7.16}$$

$$C = \begin{bmatrix} 0 & 1 & 0 & 0 \\ 0 & 0 & 0 & r \\ 0 & 0 & 0 & 1 \\ 0 & -r & 0 & 0 \end{bmatrix}, \tag{7.17}$$

and

$$d = \begin{Bmatrix} 0 \\ \cos t \\ 0 \\ \sin t \end{Bmatrix}. \tag{7.18}$$

The state of the system is then defined by the vector, y, and the vector, d, resolves the torque ratio, ν, along coordinate axes.

F. Canonical Transformation

By making the proper coordinate transformation of the state vector, y, it is possible to bring the matrix C into the simplest form. This type of transformation is quite useful in gaining an insight into the intrinsic properties of the system and simplifying the solution to the equations of motion.

Let us, therefore, introduce the new state vector, x, given by the transformation

$$y = \bar{P}x \tag{7.19}$$

where $\bar{F}$ is the modified Jordan transformation matrix (described in appendix A) for the matrix C. The Jordan transformation matrix, P, is calculated (using the method described in ref. 15) and modified to yield

$$\bar{P} = \begin{bmatrix} 1 & 0 & 1 & 0 \\ 0 & 0 & 0 & r \\ 0 & 1 & 0 & 1 \\ 0 & 0 & -r & 0 \end{bmatrix} . \tag{7.20}$$

The substitution of equations (7.19), and (7.20) into equation (7.15) leads to

$$\dot{x}(t) = Ax(t) + b(t)\, u(t) \tag{7.21}$$

where

$$A = \bar{P}^{-1} C\bar{P} = \begin{bmatrix} 0 & 0 & 0 & 0 \\ 0 & 0 & 0 & 0 \\ 0 & 0 & 0 & +r \\ 0 & 0 & -r & 0 \end{bmatrix} , \tag{7.22}$$

$$b(t) = \begin{Bmatrix} -\sin t \\ -\cos t \\ \sin t \\ \cos t \end{Bmatrix} , \tag{7.23}$$

and

$$u(t) = \frac{v(t)}{r} = \frac{M(t)}{I_a \Omega^2} \quad . \tag{7.24}$$

From equations (7.21), (7.22), and (7.23) the equations of motions can be written explicitly as

$$\begin{aligned} \dot{x}_1 &= - u \sin t, \\ \dot{x}_2 &= - u \cos t, \\ \dot{x}_3 &= r x_4 + u \sin t, \end{aligned} \tag{7.25}$$

and

$$\dot{x}_4 = - r x_3 + u \cos t.$$

We have succeeded in separating the original fourth-order system into two first order systems and a second order system; however, the control, u, now affects all parts of the system. The physical significance of canonical state vector (x) and the control variable (u) resulting from the transformation of equation (7.19) tends to become lost in the algebraic manipulation of matrices. However, in appendix B, it is shown that a definite physical meaning is attached to each of these variables.

Equations (7.25) are the simplest nondimensional, linearized set which govern the state of the system to be optimized for small values

of θ and $\frac{d\psi}{d\tau}$. The task is now to choose u so as to transform the initial state to a desired terminal state, and to use the least control fuel in doing so.

VIII. FUEL-OPTIMAL CONTROL

Having developed the state equations which govern the system motion, we shall now develop the additional equations and conditions necessary to mathematically define the subject fuel-optimal control problem. In addition, we shall discuss some of the properties of the solution relating to uniqueness and the lower bounds on fuel consumption.

A. Statement of the Problem

In a reaction jet, the rate of fuel consumption is proportional to the control magnitude, $|u|$. The control is constrained since it emanates from a single jet of a fixed size so that

$$u \in U \tag{8.1}$$

where $U = u:\{0 \leq u \leq u_{max}\}$ is a subset of the Euclidian space R_1, and u_{max} is the maximum control available. Thus, any realizable control is always positive (or zero) and $u = |u|$. A measure of the total fuel consumed is then given by the performance index

$$J(u) = \int_0^T u(t)\, dt \tag{8.2}$$

where the initial time is zero and T is a fixed final time.

Let us consider an admissible control u as one which is defined, and piecewise continuous on some interval $[0,T]$, and $u \in U$ for all $t \in [0,T]$. Further, let us choose the initial orientation of our

coordinate system so that the desired final orientation is the origin, i.e., $x(T) = 0$. The subject optimal control problem can then be formally stated as follows: For the system governed by the state equations of (7.21), find the admissible control, u, which minimizes the performance index of equation (8.2) and transfers the state of the system from $x(0) = x_0$ to $x(T) = 0$. This problem is classified as a fixed end-point problem with a fixed final time and a bounded control.

B. Necessary Conditions for Optimality

The celebrated minimum principle (or equivalent maximum principle) of Pontryagin (ref. 16) gives a very elegant method for handling the preceding problem with a bounded control variable. This minimum principle utilizes the Hamiltonian function, $H(x,p,u,t)$ given by

$$H(x,p,u,t) = p(t) \cdot \left[Ax(t) + b(t)\, u(t)\right] + u(t) \qquad (8.3)$$

where $p(t)$ is the $4x1$ costate (or adjoint) vector; the terms in brackets are the right side of equation (7.21); and the remaining u is the integrand of equation (8.2).

1. Minimum Principle - The minimum principle for our problem is given in reference 17, in the form of a theorem similar to the following:

Theorem (8-1): Let $u^*(t)$ be an admissible control which transfers the state of the system form $x(0) = x_0$ to $x(T) = 0$ where T is the fixed terminal time. Let $x^*(t)$ be the trajectory corresponding to $u^*(t)$, originating at $x^*(0) = x_0$, and terminating at $x^*(T) = 0$. In

order that u^* be optimal (for minimization of the cost function of equation (8.2)), it is necessary that there exist a function $p^*(t)$ such that

1. $p^*(t)$ corresponds to $u^*(t)$ and $x^*(t)$, so that $p^*(t)$ and $x^*(t)$ are solutions of the canonical system

$$\dot{x}^*(t) = \frac{\partial H(x^*,p^*,u^*,t)}{\partial p} \tag{8.4a}$$

and

$$\dot{p}^*(t) = -\frac{\partial H(x^*,p^*,u^*,t)}{\partial x} \tag{8.4b}$$

satisfying the boundary conditions

$$x^*(0) = x_0 \tag{8.5a}$$

and

$$x^*(T) = 0. \tag{8.5b}$$

2. The function $H(x^*,p^*,u^*,t)$ has an absolute minimum as a function of u over U at $u(t) = u^*(t)$ for t in $[0,T]$; that is

$$\min_{u \in U} H(x^*,p^*,u,t) = H(x^*,p^*,u^*,t) \tag{8.6}$$

or equivalently

$$H(x^*,p^*,u^*,t) \leq H(x^*,p^*,u,t) \tag{8.7}$$

for all u in U.

The conditions of theorem (8-1) provide only the local necessary conditions for an extremal control and, in general, are not sufficient.

2. Optimal Control Equations - If we substitute the Hamilton function of equation (8.3) into the equations of Theorem (8-1) we then obtain the differential equations

$$\dot{x}^*(t) = Ax^*(t) + b(t)\, u^*(t) \tag{8.8a}$$

and

$$\dot{p}^*(t) = - A'p^*(t) \tag{8.8b}$$

where A' is the transpose of A; the boundary conditions

$$x^*(0) = x_0 \tag{8.9a}$$

and

$$x^*(T) = 0; \tag{8.9b}$$

and the minimum condition

$$\min_{u \in U} \left[p^*(t) \cdot b(t) + 1\right] u(t) = \left[p^*(t) \cdot b(t) + 1\right] u^*(t). \tag{8.10}$$

The admissible optimal control which satisfies equation (8.10) and minimizes H is clearly

$$u^*(t) = 0 \text{ for } f_s(t) > 0$$

or

$$= u_{max} \text{ for } f_s(t) < 0 \tag{8.11}$$

where f_s is the switching function given by

$$f_s(t) = 1 + p^*(t) \cdot b(t). \tag{8.12}$$

The control of equation (8.11) can be substituted into equations (8.8) to obtain a set of eight equations in the eight dependent variables x,p of the form:

$$\dot{x}^*(t) = Ax^*(t) + b(t)\, u_{max}\, \xi(f_s) \tag{8.13a}$$

and

$$\dot{p}^*(t) = - A'p^*(t) \tag{8.13b}$$

where $\xi(f_s)$ is similar to the unit step function and is defined as

$$\xi(f_s) = 1 \text{ if } f_s < 0$$

$$= 0 \text{ if } f_s > 0.$$

With the eight boundary conditions of equation (8.9) we can, at least in theory, solve the resulting eight equations. It is noted that the boundary conditions are split, i.e., half are specified at the initial time and half at the final time. The determination of the optimal control thus reduces to the solution of a difficult nonlinear two point boundary value problem.

C. Controllability

A system is said to be controllable if the final state $x(T) = 0$ is reachable from the initial state x_0 with the control $u \in U$. Controllability is thus a necessary condition for optimality.

To establish controllability, let us turn to the solution to equation (7.21) which can be written as (ref. 17, p. 130)

$$x(t) = X(t) \left[x_0 + \int_0^t X^{-1}(t)\, b(t)\, u(t)\, dt \right] \tag{8.14}$$

where $u \in U$ and

$$X(t) = \begin{bmatrix} 1 & 0 & 0 & 0 \\ 0 & 1 & 0 & 0 \\ 0 & 0 & \cos rt & \sin rt \\ 0 & 0 & -\sin rt & \cos rt \end{bmatrix} \tag{8.15}$$

is the fundamental matrix which satisfies the equation

$$\dot{X}(t) = AX(t) \tag{8.16a}$$

with

$$X(0) = I \text{ (the identity matrix).} \tag{8.16b}$$

For all trajectories which pass through the end-point $x(T) = 0$ we have from equation (8.14) that

$$x_0 = - \int_0^T X^{-1}(t)\, b(t)\, u(t)\, dt, \; u \in U. \tag{8.17}$$

The right side of equation (8.17) is then the set of all points which can be driven to the origin with an admissible control. We can thus state that an arbitrary initial state x_0, is controllable if, and only if

$$x_0 \in \left\{ - \int_0^T X^{-1}(t)b(t)u(t)dt: \; u \in U \right\}. \tag{8.18}$$

We can show that equation (8.18) implies a more specific controllability requirement by using equations (7.23) and (8.15) in equation (8.17) to obtain

$$x_0 = - \int_0^T \begin{Bmatrix} -\sin t \\ -\cos t \\ \sin (1-r)t \\ \cos (1-r)t \end{Bmatrix} u(t)dt. \tag{8.19}$$

From the periodicity of the integrand and the bounds on u we can then state an auxiliary requirement that, for the state x_0 to be controllable, it is necessary that

$$|x_{i0}| \leq 2ju_{max} \qquad i = 1,2,3,4 \tag{8.20}$$

where x_{i0} are the components of the initial state vector, x_0, and j in an integer such that

$$\frac{T}{2\pi} \leq j \leq \frac{T}{2\pi} + 1. \tag{8.21}$$

The integer j is then the maximum number of complete periods that any of the functions of the integrand of equation (8.19) can pass through and $2u_{max}$ is the maximum value attainable in any one period.

It is noted that equations (8.18) and (8.20) only give the necessary conditions for controllability and that equation (8.18) implies equation (8.20) whereas equation (8.20) does not necessarily imply equation (8.18).

D. Singular Control

In determining the optimal control given by equation (8.11), we tacitly ignored the possibility of a singular control (i.e., the required control for $f_s(t) = 0$ over some finite interval of time). By investigating the behavior of the switching function, we shall prove that a singular control does not exist and the control problem is "normal".

In order to determine the switching function, we must first solve the differential equations for the costate variables, which can be written out explicity from equations (8.8b) and (7.22) as

$$\begin{aligned} \dot{p}_1 &= 0, \\ \dot{p}_2 &= 0, \\ \dot{p}_3 &= + rp_4, \end{aligned} \tag{8.22}$$

and

$$\dot{p}_4 = - rp_3.$$

The solutions to equations (8.22) are then

$$p_1(t) = p_{10},$$
$$p_2(t) = p_{20},$$
$$p_3(t) = p_{30} \cos rt + p_{40} \sin rt, \tag{8.23}$$

and

$$p_4(t) = - p_{30} \sin rt + p_{40} \cos rt$$

where $p_{i0} = p_i(0)$, $i = 1,2,3,4$. The substitution of equations (7.23) and (8.23) into equation (8.12) then gives

$$f_s = 1 - p_{10} \sin t - p_{20} \cos t + (p_{30} \cos rt + p_{40} \sin rt) \sin t$$
$$+ (- p_{30} \sin rt + p_{40} \cos rt) \cos t$$

or upon the use of trigonometric identities

$$f_s = 1 - p_{10} \sin t - p_{20} \cos t + p_{30} \sin(1 - r)t + p_{40} \cos (1 - r)t. \tag{8.24}$$

Equation (8.24) can be reduced further to the form

$$f_s = 1 - A_1 \sin(t + \beta_1) - A_2 \sin \left[(1 - r)t + \beta_2\right] \tag{8.25}$$

where

$$A_1 = \sqrt{p_{10}^2 + p_{20}^2}, \tag{8.26}$$

$$\beta_1 = \tan^{-1}(p_{20}/p_{10}), \tag{8.27}$$

$$A_2 = \sqrt{p_{30}^2 + p_{40}^2}, \tag{8.28}$$

and

$$\beta_2 = \tan^{-1}(-p_{40}/-p_{30}). \tag{8.29}$$

The switching function of equation (8.25) which results from the superposition of two quantities of different frequencies gives rise to a "beating" phenomenon. This is shown (for $r < 1$) by writing equation (8.25) as

$$f_s = 1 - \Big\{\left[A_1 \cos(rt + \beta_1 - \beta_2) + A_2\right] \sin\left[(1 - r)t + \beta_2\right] + A_1 \sin(rt + \beta_1 - \beta_2) \cos\left[(1 - r)t + \beta_2\right]\Big\}$$

or upon reduction as

$$f_s = 1 - D(t) \sin\left[(1 - r)t + \beta_2 + \delta(t)\right] \tag{8.30}$$

where the amplitude $D(t)$ is

$$D(t) = \sqrt{A_1^2 + A_2^2 + 2A_1A_2 \cos(rt + \beta_1 - \beta_2)} \tag{8.31}$$

and the time varying phase angle $\delta(t)$ is

$$\delta(t) = \tan^{-1}\left[\frac{\sin(rt + \beta_1 - \beta_2)}{\cos(rt + \beta_1 - \beta_2) + A_2/A_1}\right]. \qquad (8.32)$$

From equation (8.31) the amplitude $D(t)$ is seen to vary periodically at the frequency r (the nutation frequency) with

$$D_{max} = A_1 + A_2 \qquad (8.33)$$

and

$$D_{min} = A_1 - A_2$$

A similar approach can be taken for $r > 1$ however, the amplitude of D varies at the frequency $(2 - r)$. A plot of the switching function of equation (8.30) versus time would then similar to figure 8.1 (for $r < 1$).

Clearly, from either equation (8.30) or figure 8.1 it is seen that because of its periodic nature, the switching function can never be zero over any finite time interval. The possibility of a singular control, thus, does not exist. The fuel-optimal control is then a piecewise constant function of time which switches between 0 and u_{max} at a finite number of times. By definition, problems leading to such a control are called " normal" control problems.

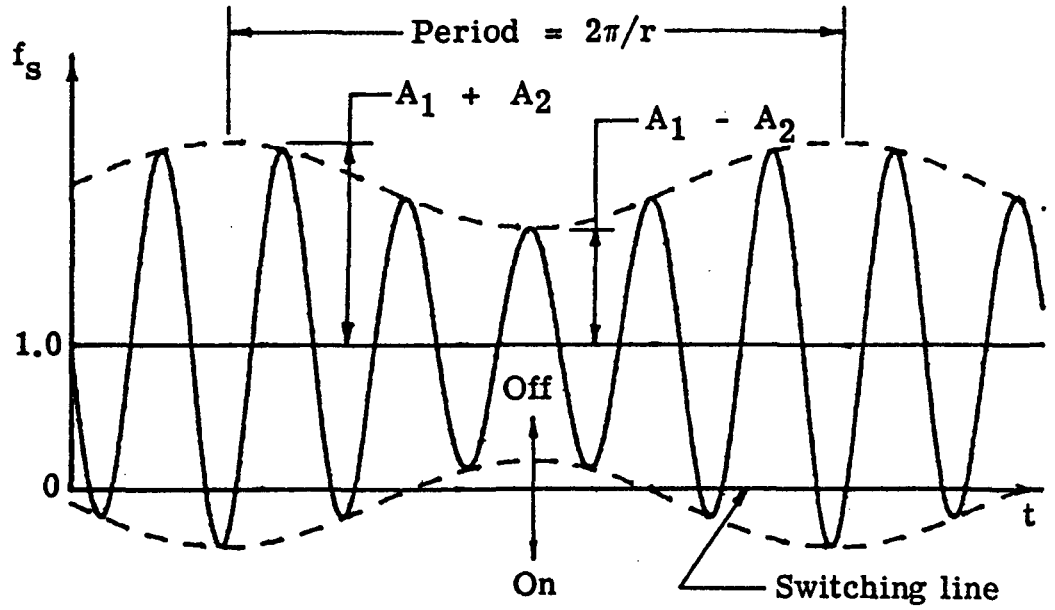

Figure 8.1.- Switching function behavior.

E. Uniqueness of Optimal Control

In general, more than one optimal control may exist for a given initial and final state. However, it follows from the definition of fuel-optimality that the minimum fuel is unique. It is shown in the following that because of the "normality" of the subject problem that the fuel-optimal control (if it exists) is also unique.

To prove the uniqueness, let us suppose that $u^*(t)$ and $\tilde{u}^*(t)$ are two distinct fuel-optimal controls transferring the intial state x_0 to the origin in the same time T. Let $x^*(t)$ and $\tilde{x}^*(t)$ be the distinct trajectories originating at x_0. Since both $u^*(t)$ and $\tilde{u}^*(t)$ are assumed to be fuel-optimal, we have the relation (from the performance index of equation (8.2))

$$\int_0^T u^*(t)dt = \int_0^T \tilde{u}^*(t)dt. \tag{8.34}$$

Now the solutions of $x^*(t)$ and $\tilde{x}^*(t)$ are given by equation (8.14) as

$$x^*(t) = X(t)\left[x_0 + \int_0^t X^{-1}(t)b(t)u^*(t)dt\right] \tag{8.35}$$

and

$$\tilde{x}^*(t) = X(t)\left[x_0 + \int_0^t X^{-1}(t)b(t)\tilde{u}^*(t)dt\right]. \tag{8.36}$$

At $t = T$, we must have the terminal condition

$$x^*(T) = \tilde{x}^*(T) = 0 \tag{8.37}$$

and so we deduce that the (vector) equality

$$\int_0^T X^{-1}(t)b(t)u^*(t)dt = \int_0^T X^{-1}(t)b(t)\tilde{u}^*(t)dt \tag{8.38}$$

holds. Let $p^*(t)$ be the costate corresponding to the fuel optimal trajectory $x^*(t)$. Let $p^*(0) = p_0^*$, so that we may write the solution to equation (8.8b) as (ref. 17, p. 147)

$$p^{*\prime}(t) = p_0^{*\prime} X^{-1}(t) \tag{8.39}$$

where the prime denotes the transpose. From the necessary conditions of equation (8.10) we know that

$$\left[p^*(t) \cdot b(t) + 1\right] u^*(t) \leq \left[p^*(t) \cdot b(t) + 1\right]\tilde{u}^*(t) \tag{8.40}$$

because equation (8.10) holds for all $u(t)$ and, in particular, for $\tilde{u}^*(t)$. We have assumed that $u^*(t)$ and $\tilde{u}^*(t)$ are distinct and since the fuel-optimal problem is normal, the inequality in equation (8.40) is strict whenever

$$\tilde{u}^*(t) \neq u^*(t) \tag{8.41}$$

For this reason, the relation of equation (8.40) reduces to the strict inequality

$$\left[p^*(t) \cdot b(t) + 1\right]u^*(t) < \left[p^*(t) \cdot b(t) + 1\right]\tilde{u}^*(t) \qquad (8.42)$$

whenever equation (8.41) holds.

If we integrate both sides of equation (8.42), we find that (for distinct $u^*(t)$ and $\tilde{u}^*(t)$)

$$\int_0^T \left[p^*(t) \cdot b(t) + 1\right] u^*(t)dt < \int_0^T \left[p^*(t) \cdot b(t) + 1\right]\tilde{u}^*(t)dt \qquad (8.43)$$

and that [in view of equation (8.34)]

$$\int_0^T p^*(t) \cdot b(t)u^*(t)dt < \int_0^T p^*(t) \cdot b(t)\tilde{u}^*(t)dt. \qquad (8.44)$$

Now let us premultiply equation (8.38) by $p_0^{*\prime}$ to obtain

$$p_0^{*\prime} \int_0^T X^{-1}(t)b(t)u^*(t)dt = p_0^{*\prime} \int_0^T X^{-1}(t)b(t)\tilde{u}^*(t)dt. \qquad (8.45)$$

Since $p_0^{*\prime}$ is a constant vector we then can use (8.39) to reduce (8.45) to

$$\int_0^T p^*(t) \cdot b(t)u^*(t)dt = \int_0^T p^*(t) \cdot b(t)\tilde{u}^*(t)dt. \qquad (8.46)$$

Thus, the assumption that u^* and $\tilde{u}^*$ are distinct and full-optimal has led to the two relations equation (8.44) and equation (8.46), which are contradictory. It then follows that $u^*(t) = \tilde{u}^*(t)$ for all $t \in [0,T]$ (except possible at the switch times), and so the fuel-optimal control is unique.

F. Lower Bound on Minumum Fuel

In seeking the fuel-optimal control, it is quite useful to establish the lower bound on the fuel requirement. That is, what is the best we could possible do?

To answer this question let us refer to equation (8.19). If, as in appendix B, we define the initial momentum and nutation vector quantities

$$h_0 = (x_{10}, x_{20}) \tag{8.47}$$

and

$$n_0 = (x_{30}, x_{40}) \tag{8.48}$$

then we can write equation (8.19) in partioned form as

$$h_0 = \int_0^T \begin{Bmatrix} \sin t \\ \cos t \end{Bmatrix} u(t)dt \tag{8.49}$$

and

$$n_0 = -\int_0^T \begin{Bmatrix} \sin(1-r)t \\ \cos(1-r)t \end{Bmatrix} u(t)dt. \tag{8.50}$$

From equation (8.49) we see that

$$|h_d| \leq \int_0^T \left| \begin{Bmatrix} \sin t \\ \cos t \end{Bmatrix} u(t) \right| dt = \int_0^T u(t)dt. \tag{8.51}$$

Thus, from equations (8.2) and (8.51) we have

$$J(u) \geq |h_d| . \tag{8.52}$$

Physically, equation (8.52) states that the total moment impulse is greater than the magnitude of the initial angular momentum vectors. In view of impulse momentum theory this result is intuitively obvious.

By proceeding in a similar manner we obtain from equation (8.50)

$$J(u) \geq |n_0| . \tag{8.53}$$

The lower bound on $J(u)$ is then given by the larger of equations (8.52) or (8.53). That is

$$(x_{10}^2 + x_{20}^2)^{1/2} \leq J(u) \geq (x_{30}^2 + x_{40}^2)^{1/2}. \tag{8.54}$$

Equation (8.54) provides an important property of the optimal control. That is, for a limited amount of fuel, only certain initial conditions can be controlled.

IX. SOLUTION OF THE BOUNDARY VALUE PROBLEM

Determination of the fuel-optimal control has led (via the minimum principle) to eqs. (8.13), a two-point-nonlinear-boundary value problem, which is unsolvable in closed form. A similar situation arises in most optimization problems, We must, therefore, resort to a numerical solution. Numerical integration, however, requires that all boundary data be given at the same point in time. Computation of the solution, thus, necessitates an iterative procedure in which the unknown initial costate vector is assumed, the integration carried out, and an attempt made to match the given end conditions. The solution difficulties are compounded by the discontinuous nature of the control, which (as illustrated in fig. 8.1) tends toward an impulse and has many switches.

Numerous general techniques have been developed for solutions to two-point boundary-value problems (see ref. 18); however, most are either not applicable or difficult and inefficient to apply to the present bounded control problem. The one exception is a relatively unknown method due to Neustadt (ref. 19). Neustadt's method involves the maximization of an augmented performance index by some type of gradient search. The outstanding feature of this approach is that the gradient can be simply determined in closed form and need not be generated numerically.

In the derivation of his method, Neustadt employed geometrical arguments which are unfamiliar to many control practitioners. In the following, a variation of Neustadt's method is derived directly from

the minimum principle. A computational algorithm utilizing the augmented performance index and its gradient is then incorporated into a digital computer program to yield the desired solution. This is the first-known application of this method to a practical problem.

A. Augmented Performance Index

Before proceeding with the computational algorithm, we shall define the augmented performance index and its properties by theorem (9-1) and its gradient by theorem (9-2). The corresponding proofs follow.

Theorem 9-1: Let $x(p_0,t)$ and $p(p_0,t)$ be the solutions to eqs. (8.13) with the initial conditions $x(0) = x_0$ and $p(0) = p_0$ (an arbitrary initial vector), and let $u(p_0,t)$ be the corresponding admissible control given by eq. (8.11). Also, let $J(u^*) = \int_0^T u^*(t)dt$ be the minimum performance index corresponding to the desired optimal control $u^*(t)$ which transfers the initial state from $x^*(0) = x_0$ to the final state $x^*(T) = 0$. Then, the augmented performance index given by

$$\bar{J}(p_0) = J\left[u(p_0)\right] + p(p_0,T) \cdot x(p_0,T) \tag{9.1}$$

must satisfy the maximum condition

$$\max_{p_0} \bar{J}(p_0) = J(u^*) \tag{9.2}$$

or equivalently,

$$\bar{J}(p_0) \leq J(u^*) \tag{9.3}$$

where the strict equality holds if, and only if, $p_0 = p_0^*$ in which case

$$\begin{aligned} u(p_0^*,t) &= u^*(t), \\ x(p_0^*,t) &= x^*(t), \end{aligned} \tag{9.4}$$

and

$$p(p_0^*,t) = p^*(t).$$

Proof: From the minimum principle given by eq. (8.10) we know that

$$(p^*(t) \cdot b(t) + 1)u^*(t) \leq (p^*(t) \cdot b(t) + 1)u(t), \quad u \in U. \tag{9.5}$$

Since the endpoints of the state variables are fixed, the initial conditions on the costate variable are unknown. If we arbitrarily assume the initial conditions $p(0) = p_0$ and choose an admissible control in accordance with the minimum principle [eq. (8.11)], it is clear that we generate an admissible optimal control $u(p_0,t)$ which transfers the desired initial state, $x(0) = x_0$, to an undesired final state, $x(p_0,T)$. For this control, the equivalent of equation (9.5) is

$$(p(p_0,t) \cdot b(t) + 1)u(p_0,t) \leq (p(p_0,t) \cdot b(t) + 1)\tilde{u}(t) \tag{9.6}$$

where $\tilde{u}(t)$ is an arbitrary admissible control vector. If we choose $\tilde{u}(t) = u^*(t)$ (the optimal control to the desired endpoint $x^*(T) = 0$) and integrate equation (9.6) over the interval $[0,T]$ we obtain

$$\int_0^T (p(p_0,t) \cdot b(t) + 1)u(p_0,t)dt \leq \int_0^T (p(p_0,t) \cdot b(t) + 1)u^*(t)dt \tag{9.7}$$

The costate vector given by the solution of equation (8.8b) with the initial conditions $p(0) = p_0$ is (see eq. (8.39))

$$p'(p_0,t) = p_0' X^{-1}(t). \tag{9.8}$$

From equations (8.2) and (9.8), equation (9.7) becomes

$$p_0' \int_0^T X^{-1}(t)b(t)u(t)dt + J\left[u(p_0)\right] \leq p_0' \int_0^T X^{-1}(t)b(t)u^*(t)dt + J(u^*) \tag{9.9}$$

which by equation (8.14) reduces to

$$p_0'(X^{-1}(T)x(p_0,T) - x_0) + J\left[u(p_0)\right] \leq p_0'(X^{-1}(T)x^*(T) - x_0) + J(u^*) \tag{9.10}$$

or since $x^*(T) = 0$

$$p_0' X^{-1}(T)x(p_0,T) + J\left[u(p_0)\right] \leqq J(u^*). \tag{9.11}$$

Finally, the substitution of equation (9.8) into equation (9.11) gives

$$\bar{J}(p_0) = J\left[u(p_0)\right] + p(p_0,T) \cdot x(p_0 \cdot T) \leq J(u^*) \tag{9.12}$$

which proves equations (9.2) and (9.3). Further, it is clear that the left side of equation (9.12), $\bar{J}(p_0)$, is equal to the right side if, and only if, $x(p_0,T) = x^*(T) = 0$ in which case $p_0 = p_0^*$, and $u = u^*$ and we have equation (9.4).

Theorem 9-2: The gradient of the function $\bar{J}(p_0)$ given by equation (9.1) in theorem (9-1) is

$$\frac{\partial \bar{J}(p_0)}{\partial p_0} = X^{-1}(T)x(p_0,T). \tag{9.13}$$

Proof: Let us assume that $\tilde{p}_0$ is a small variation in the initial costate vector p_0 such that

$$\tilde{p}_0 = p_0 + \Delta p_0. \tag{9.14}$$

Then, in view of equations (9.1) and (9.8) we can write

$$\bar{J}(\tilde{p}_0) = \tilde{p}_0' X^{-1}(T)\tilde{x}(\tilde{p}_0,T) + J\left[\tilde{u}(\tilde{p}_0)\right] \tag{9.15}$$

and

$$\bar{J}(p_0) = p_0' X^{-1}(T)x(p_0,T) + J\left[u(p_0)\right]. \tag{9.16}$$

Subtracting equation (9.16) from equation (9.15) yields

$$\Delta\bar{J} = \tilde{p}_0 X^{-1}(T)\tilde{x}(\tilde{p}_0,T) - p_0' X^{-1}(T)x(p_0,T) + \Delta J \tag{9.17}$$

where $\Delta\bar{J}$ and ΔJ are the changes corresponding to the incremental change Δp_0.

Equation (9.17) can then be rearranged so that

$$\Delta\bar{J} = (\tilde{p}_0' - p_0')X^{-1}(T)x(p_0,T) + \tilde{p}_0' X^{-1}(T)\left[\tilde{x}(\tilde{p}_0,T) - x(p_0,T)\right] + \Delta J$$

or using equation (9.14)

$$\Delta\bar{J} - \Delta p_0' X^{-1}(T)x(p_0,T) = \Delta p_0' X^{-1}(T)\Delta x + p_0' X^{-1}(T)\Delta x + \Delta J \tag{9.18}$$

where $\Delta x = \tilde{x} - x$. It then follows (from a Schwartz inequality condition) that

$$\left| \Delta\bar{J} - \Delta p_0' X^{-1}(T)x(p_0,T) \right| \leq \left| \Delta p_0' X^{-1} \Delta x \right| + \left| p_0' X^{-1}(T)\Delta x + \Delta J \right| \quad (9.19)$$

Starting with equation (9.6), we can derive an equation similar to equation (9.11) which is

$$p_0' X^{-1}(T)x(p_0,T) + J\left[u(p_0)\right] \leq p_0' X^{-1}(T)\tilde{x}(\tilde{p}_0,T) + J\left[\tilde{u}(\tilde{p}_0,T)\right] \quad (9.20)$$

or by interchanging the roles of p_0 and $\tilde{p}_0$

$$\tilde{p}_0' X^{-1}(T)\tilde{x}(\tilde{p}_0,T) + J\left[\tilde{u}(\tilde{p}_0)\right] \leq \tilde{p}_0' X^{-1}(T)x(p_0,T) + J\left[u(p_0,T)\right]. \quad (9.21)$$

Equations (9.20) and (9.21) can be rearranged to give

$$p_0' X^{-1}(T)\Delta x + \Delta J \geq 0 \quad (9.22)$$

and

$$- p_0' X^{-1}(T)\Delta x - \Delta J \geq 0. \quad (9.23)$$

Since the sum of two positive quantities is greater than either we see that the sum of equations (9.22) and (9.23) is greater than equation (9.22) or

$$- \Delta p X^{-1}(T)\Delta x \geq p_0' X^{-1}(T)\Delta x + \Delta J \geq 0. \quad (9.24)$$

Then it follows that

$$\left| \Delta p X^{-1}(T)\Delta x \right| \geq \left| p_0' X^{-1}(T)\Delta x + \Delta J \right|. \quad (9.25)$$

Now substituting equation (9.25) into equation (9.19) gives

$$\left| \Delta\bar{J} - \Delta p_0' X^{-1}(T)x(p_0,T) \right| \leq 2\left| \Delta p_0' X^{-1}(T)\Delta x \right|. \quad (9.26)$$

The right side of equation (9.26) involves products of differentials and is of higher order than the left side. Therefore, in the limit as $\Delta p_0 \to 0$, equation (9.26) becomes

$$\left| d\bar{J}(p_0) - dp_0' X^{-1}(T) x(p_0,T) \right| \leq \left| 0 \right|$$

which leads to

$$d\bar{J}(p_0) = dp_0' X^{-1}(T) x(p_0,T). \tag{9.27}$$

Now by definition

$$d\bar{J}(p_0) = dp_0' \frac{\partial \bar{J}}{\partial p_0}(p_0). \tag{9.28}$$

Then subtracting equation (9.27) from equation (9.28) we have

$$\frac{\partial \bar{J}(p_0)}{\partial p_0} = X^{-1}(T) x(p_0,T) \tag{9.29}$$

and thus the proof of equation (9.13).

B. Computational Algorithm

An iterative procedure for solving the two-point boundary value problem through the use of theorems (9-1) and (9-2) will now be described. First we guess an initial value of p_0 and determine from equations (8.11) and (8.25) the admissible control $u(p_0,t)$ which minimizes the Hamilitonian. Using this control, the performance function $J\left[u(p_0)\right]$ is determined from equation (8.2), and the state equation (8.8a) is

integrated to obtain the final state $x(p_0,T)$. Next, the auxiliary performance function, $\bar{J}(p_0)$, given by equation (9.1) is calculated. Then, using the gradient given by equation (9.13) and a gradient search technique, we determine a new value of p_0. The whole process is then repeated until we iteratively maximize the function $\bar{J}(p_0)$ in accordance with equation (9.2). The resulting control is the optimal control and the maximum value of $\bar{J}(p_0)$ is the minimum value of $J(u)$ (i.e., $J(u^*)$).

1. Iterative Gradient Search - When the gradient of the performance function is defined analytically, the method of Fletcher and Powell (ref. 20) is probably the most powerful general procedure for finding a local minimum which is presently known. Accordingly, this method is adopted herein. The Fletcher-Powell (FP) method is not plagued with the convergence problems that exist in most other methods since it always converges and it converges rapidly. In order to apply it to our problem we merely reverse the sign on the augmented performance function and its gradient. That is the minimization of $-\bar{J}(p_0)$ is equivalent to the maximization of $\bar{J}(p_0)$.

The FP method makes use of the fact that the direction in which a function decreases most rapidly is opposite to the direction of the gradient. Hence, for the first-order Taylor series expansion of a scalar quantity $f(z + \Delta z)$ (where z is an n dimensional vector) about z we have

$$f(z + \Delta z) \approx f(z) + \frac{\partial f(z)}{\partial z} \cdot \Delta z. \tag{9.30}$$

If we choose Δz to be

$$\Delta z = ks \tag{9.31}$$

where k is a positive constant and s is a direction proportional to the negative of the gradient, i.e.,

$$s = - Wg \tag{9.32}$$

with W being a $n \times n$ positive definite weighting matrix and g the gradient given by

$$g = \frac{\partial f(z)}{\partial z} \tag{9.33}$$

then equation (9.30) becomes

$$f(z + ks) = f(z) - kg'Wg. \tag{9.34}$$

Clearly, if k is small enough so that equation (9.30) holds, then

$$f(z + ks) < f(z). \tag{9.35}$$

The fundamental basis of the FP method is that for each iteration k is obtained such that $f(z + k^*s)$ is a minimum with respect to k along $z + ks$. The FP method is thus on "optimum step" gradient method. The procedure for obtaining the minimum along a line is not central to the method; but, it is precisely this procedure which establishes the efficiency of the method in terms on the number of function and gradient evaluation required for convergence. The "optimal step" search procedure used herein is discussed in the following section.

The weighting matrix W in the FP method is initially chosen to be an arbitrary positive definite matrix. It is then updated after each iteration step according to the equations.

$$W^{i+1} = W^i + G^i + H^i \tag{9.36}$$

where i denotes the ith iteration step,

$$G^i = \frac{\Delta z \, \Delta z'}{\Delta z' v}, \tag{9.37}$$

and

$$H^i = - \frac{(W^i v)(W^i v)'}{v' W^i v} \tag{9.38}$$

with

$$v = g^{i+1} - g^i \tag{9.39}$$

and

$$\Delta z = k^{*i} s^i .$$

As the procedure converges, W tends to $\left(\frac{\partial^2 f(z)}{\partial z_i \partial z_j}\right)^{-1}$, the Newton-Raphson weighting matrix (ref. 18), evaluated at the minimum. Thus, if we use the suggested initial choice of the identity matrix for W, the procedure starts out as an optimal steepest descent method and gradually changes to the Newton-Raphson method as we approach the solution.

It is shown in reference 20 that if f is of the quadratic form

$$f = f_0 + \sum_{i=1}^{n} a_i z_i + \frac{1}{2} \sum_{i=1}^{n} \sum_{j=1}^{n} R_{ij} z_i z_j \tag{9.40}$$

then the minimum is found in exactly n iterations. Accordingly, convergence is also rapid for other functions which can be locally approximated as a quadratic function.

2. Optimal Step Search - The procedure for carrying out a one-dimensional search along a line is the distinguishing feature between most "optimal step" gradient search methods. Each trial value of k in the search requires an evaluation of the function to be minimized as well as its gradient. This entails an integration of the system equations of motion over the interval $[0,T]$ for each trial. It thus behooves us to utilize a procedure which requires as few steps as possible while still maintaining an acceptable accuracy in the determination of the optimum step, k^*.

In the appendix of reference 20, a simple algorithm involving cubic interpolation was given for estimating k^*. Specifically, if $f_1 = f(z_1)$, $g_1 = g(z_1)$, $f_2 = f(z_1 + k_1 s)$ and $g_2 = g(z_1 + k_1 s)$ are known numerically, then the function $f(z_1 + ks)$ in the direction of s may be approximated by the cubic

$$f(z_1 + ks) = a_0 + a_1 k + a_2 k^2 + a_3 k^3 \tag{9.41}$$

Values of the coefficients are found to be

$$\begin{aligned} a_0 &= f_1, \\ a_1 &= g_1 \cdot s, \\ a_2 &= -\frac{1}{k_1}(Z + g_{11} \cdot s), \\ a_3 &= \frac{1}{3k_1^2}\left[2Z + g_1 \cdot s + g_2 \cdot s\right], \end{aligned} \tag{9.42}$$

and

$$Z = \frac{3}{k_1}(f_1 - f_2) + g_1 \cdot s + g_2 \cdot s.$$

When equation (9.41) is differentiated with respect to k, and the result is set to zero, the minimizing value of $k = k^*$ is found to be

$$k^* = \frac{1}{3a_3}\left[-a_2 + (a_2^2 - 3a_1a_3)^{1/2}\right]. \tag{9.43}$$

A recommended initial choice of k_1 to determine f_2 and g_2 is given in reference 20 (and attributed to Davidson, ref. 21) as

$$k_1 = \text{minimum of } \left\{1, -2(f_1 - f_{min})/g_1 \cdot s\right\} \tag{9.44}$$

where f_{min} is the predicted lower bound of $f(z)$. It is noted that when s is in the Newton-Raphson direction $\left(\text{i.e., } s = -\left(\frac{\partial^2 f(z_1)}{\partial z_i \partial z_j}\right)^{-1} g(z_1)\right)$ the second term in the bracket of equation (9.44) becomes unity.

The author experienced several numerical difficulties with the above procedure, which shall be noted, and found it expedient to make

several modifications. In reference 20 it was recommended that one should ensure that the minimum is located between f_1 and f_2 by testing the sign of $g_2 \cdot s$ before interpolating. It was found that equation (9.43) is not very efficient for bounding the minimum and, likewise, neither is repeated use of equation (9.44). An extrapolation procedure is, thus, introduced to rapidly bound the minimum from above. This extrapolation procedure searches for a value equal to f_1 on the upper side of the minimum as shown in figure 9.1.

To find the extrapolated value of k we first try cubic extrapolation based on equations (9.41) and (9.42). A sketch of $f(z_1 + ks)$ as given by equation (9.41) is shown in figure 9.2.

It is seen that for $a_3 > 0$ we have a well-defined minimum, however, for $a_3 < 0$ cubic extrapolation breaks down. For the latter case we then employ parabolic extrapolation using f_1, f_2, and g_2 in which $f(z_1 + ks)$ is approximated by

$$f(z_1 + ks) = a_0 + a_1 k + \bar{a}_2 k^2. \tag{9.45}$$

The values of a_0 and a_1 are found to be the same as those of equation (9.42) but a_2 is replaced by

$$\bar{a}_2 = \frac{f_2 - f_1 - k_1 a_1}{k_1^2}. \tag{9.46}$$

The extrapolation formula are then

$$k = \left[- a_2 + \sqrt{a_2^2 - 4a_1 a_3} \right] \Big/ 2a_3 \quad \text{for} \quad a_3 > 0 \tag{9.47}$$

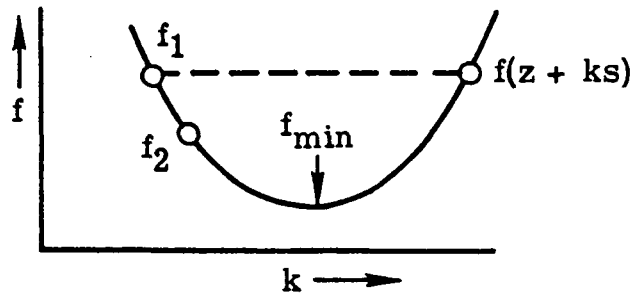

Figure 9.1.- Extrapolation search.

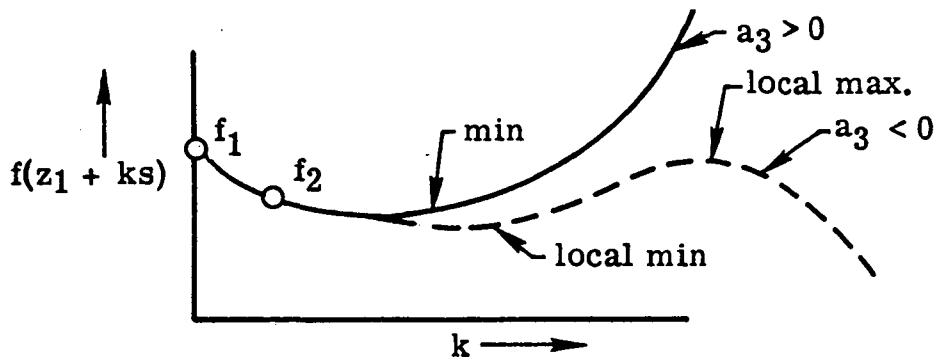

Figure 9.2.- Behavior of cubic fit.

where a_1, a_2, and a_3 are given by equation (9.42) and

$$k = - a_1/\bar{a}_2 \quad \text{for } a_3 < 0 \tag{9.48}$$

where a_1 is given by equations (9.42) and $\bar{a}_2$ by equation (9.46).

The ideal situation would be for the initial choice of k_1 obtained from equation (9.44) to bound the minimum so that extrapolation would not be necessary. In this respect, equation (9.44) becomes increasingly worse as we near the solution. Equation (9.44) was, therefore, modified so that

$$k_1 = \text{minimum of } \{K, - 2(f_1 - f_{min})/g_1 \cdot s\}. \tag{9.49}$$

The value of K is chosen to be 1 initially and self-adjusting thereafter. The adjustments are made as follows:

1. If the minimum is not bounded in the first try when searching along a given direction, s^i, we set $K = K + \Delta K$ for the next iteration direction s^{i+1}.

2. If the minimum is bounded in the first try when searching along a given direction, s^i, and $f_2 > f_1$, we set $K = K - \Delta K$ for the next iteration direction s^{i+1}. Otherwise, the value of K remains constant.

A value of $\Delta K = 0.2$ has proved to work well and minimizes oscillations in K. In practice, the general trend has been for K to gradually increase so that the minimum is nearly always bounded in the first step.

Once the minimum is bounded, we then use equation (9.43) for $a_3 > 0$ or the parabolic counterpart from equation (9.45).

$$k^* = - a_2/2\bar{a}_1 \qquad (9.50)$$

for $a_3 \leq 0$.

3. Fletcher-Powell Digital Computer Subroutine - The FLEtcher-POWell gradient search procedure mentioned above and outlined in reference 20, along with the above optimal step search have been incorporated into a general minimization subroutine entitled "FLEPOW." The value of the FunCtioN, f(z), and its GRADient, g(z), are determined in a dummy subroutine "FCNGRAD" which is supplied by the user, For the subject analysis, FCNGRAD contains the equations dictated by theorems 9-1 and 9-2.

The subroutine "FLEPOW" has been checked out on a number of problems and shown to require about 2-3 function and gradient evaluations per iteration step. Other optimal step methods generally require many more (typically 8-10). The present method, thus, indicates a trend of high efficiency.

C. Numerical Determination of the Augmented Performance Function and Its Gradient

As mentioned in the preceding section, the function, $\bar{J}(p_0)$, and its gradient, $\partial\bar{J}(p_0)/\partial p_0$, are calculated in the subroutine, FCNGRAD. Each function evaluation requires integration of the eight simultaneous equations (8.13) from the initial to the final time. The gradient of the function, however, is a closed-form function of the terminal conditions and easily obtained.

Experience has shown that numerical integration for spinning vehicles is extremely slow because a small integration step is required for even moderate spin rates. Numerical integration problems are also compounded by the bang-bang nature of the controls and sophisticated logic has to be developed to close on and cross the switch times. In an effort to avoid these numerical difficulties the numerical integration is accomplished in two phases. In the first phase a search is made to determine the switch times using large time steps, and, in the second phase a recurrence closed-form integration between the switch times is used to obtain the complete integration over the time interval $[0,T]$. The logic and equations used in each of these phases is discussed in the following.

1. Determination of Switching Times - A subroutine entitled "TSWITCH" has been written to search for the switch times associated with the switching function given by equation (8.25). This subroutine allows a large search interval nearly equal to half the minimum period of oscillation because the search logic utilizes both $\dot{f}_s$ and f_s at each step.

To search for the switch times the program starts at $t = 0$ and successively computes values of $\dot{f}_s$ and f_s at Δt intervals until a zero crossing is detected. The two types of crossings that are possible are labeled type "A" and type "B" and are shown on figures 9.3 and 9.4, respectively, along with the logic which detects them.

For a type "A" crossing the switch time is determined from a parabolic interpolation using f_1, $\dot{f}_1$, and f_2. That is

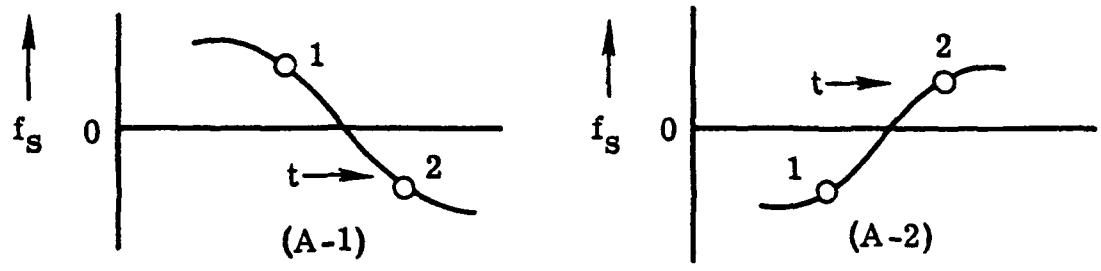

Figure 9.3.- Type "A" crossings ($f_{s_2}/f_{s_1} < 0$).

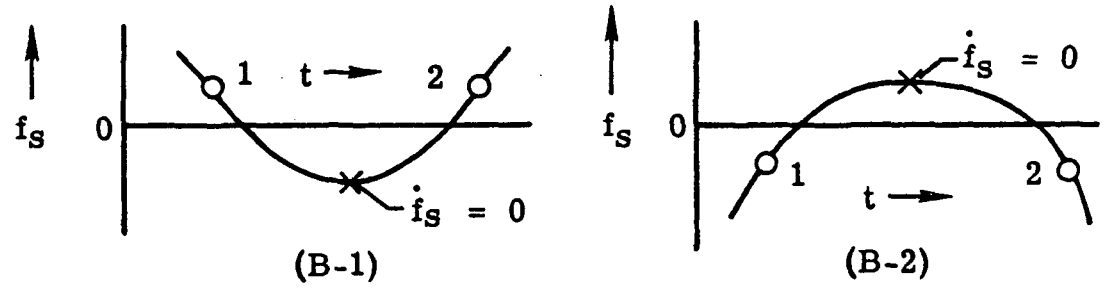

Figure 9.4.- Type "B" crossings ($f_{s_1}/f_{s_2} < 0$ and $f_{s_1}/\dot{f}_{s_1} < 0$).

$$t_{switch} = t_1 - \frac{a_1 \pm \sqrt{a_1^2 - 4a_1a_2}}{2a_2} \tag{9.51}$$

where the sign of the radical is chosen so that

$$t_1 < t_{switch} < t_2, \tag{9.52}$$

$$\begin{aligned} a_0 &= f_{s_1}, \\ a_1 &= \dot{f}_{s_1}, \\ a_2 &= (f_{s_2} - f_{s_1} - \dot{f}_{s_1}\,\Delta t)/\Delta t^2, \end{aligned} \tag{9.53}$$

and

$$\Delta t = t_2 - t_1.$$

The type "B" crossings are changed into a type "A" crossing by parabolic interpolation for the time where $\dot{f}_s = 0$ (see fig. 9.4) and replacement of the original point 2 with this point. The interpolation equation is

$$t\Big|_{\dot{f}_s=0} = t_1 - a_1/2a_2$$

where a_1 and a_2 are given by equations (9.53).

It should be noted that false type "B" crossings are indicated by the curves illustrated in figure 9.5. The fact that these are false crossings is discovered when the sign of the function at $\dot{f}_s = 0$ has the same sign as f_1. No interpolation is performed and the search continues.

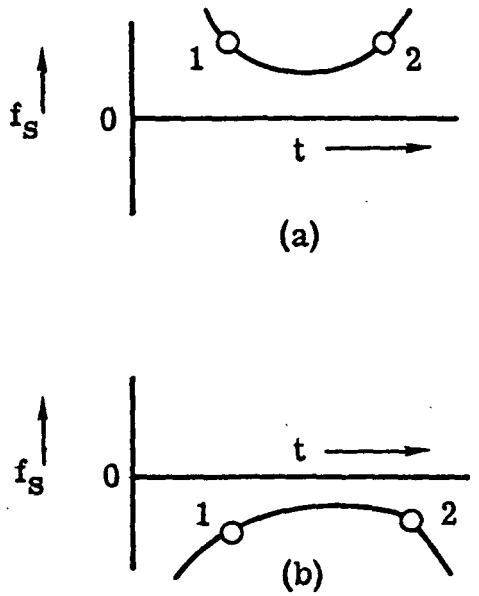

Figure 9.5.- False type "B" crossings ($\dot{f}_{s_1}/\dot{f}_{s_2} < 0$ and $f_{s_1}/\dot{f}_{s_1} < 0$).

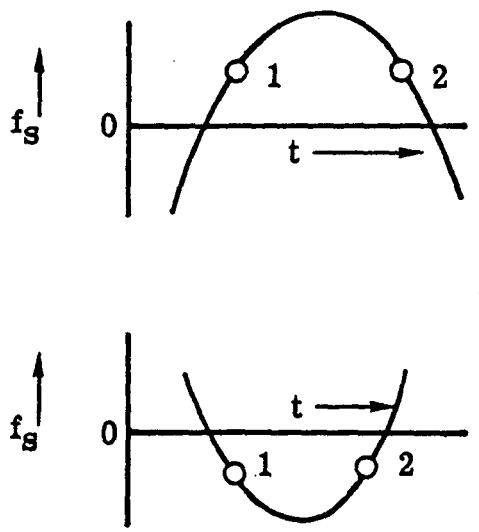

Figure 9.6.- Slope change configurations ($\dot{f}_{s_1}/\dot{f}_{s_2} < 0$).

It should also be noted that the requirement of $f_{s_1}\dot{f}_{s_1} < 0$ for a crossing in addition to the slope change requirement $\dot{f}_{s_1}/\dot{f}_{s_2} < 0$ eliminates consideration of the cases shown in figure 9.6.

The interpolation on type "A" crossings is repeated until

$$\left| \frac{t^{i+1}_{switch} - t^{i}_{switch}}{t^{i+1}_{switch}} \right| < \epsilon$$

where i and $i+1$ correspond to the last two calculated crossing times and ϵ is an error criteria. After a t_{switch} value is found the search then starts over beginning with the known point 2 on the other side of the crossing and continues until $t = T$.

The subroutine "TSWITCH" is a very efficient general search routine for periodic type functions for which a closed form derivative of the switching function exists.

2. Integration of the System Equation - A subroutine entitled "CALC" has been written to integrate the equation of motion and the performance function, $J(u)$, between the successive switch times t_i and t_{i+1}. The closed-form integral is obtained by writing equation (8.14) for the two times t_i and t_{i+1} as

$$x(t_i) = X(t_i)(x_0 + \int_0^{t_i} X^{-1}(t)b(t)u(t)dt) \qquad (9.54)$$

and

$$x(t_{i+1}) = X(t_{i+1})(x_0 + \int_0^{t_{i+1}} X^{-1}(t)b(t)u(t)dt). \qquad (9.55)$$

Solving equation (9.54) for x_0 and substituting into equation (9.55) gives

$$x(t_{i+1}) = X(t_{i+1})(X^{-1}(t_i)x(t_i) + \int_{t_i}^{t_{i+1}} X^{-1}(t)b(t)u(t)dt) \quad (9.56)$$

Finally substituting equations (7.23) and (8.15) into equation (9.56) and noting that $u(t)$ is a constant between successive switch times leads to the explicit recurrence equations.

$$\begin{aligned}
x_1(t_{i+1}) &= x_1(t_i) + u(\cos t_{i+1} - \cos t_i), \\
x_2(t_{i+1}) &= x_2(t_i) - u(\sin t_{i+1} - \sin t_i), \\
x_3(t_{i+1}) &= R \cos r\,\Delta t + S \sin r\,\Delta t - \frac{u}{1 - r} \cos t_{i+1}, \\
x_4(t_{i+1}) &= - R \sin r\,\Delta t + S \cos r\,\Delta t + \frac{u}{1 - r} \sin t_{i+1}, \\
R &= x_3(t_i) + \frac{u}{1 - r} \cos t_i, \\
S &= x_4(t_i) - \frac{u}{1 - r} \sin t_i,
\end{aligned} \quad (9.57)$$

and

$$\Delta t = t_{i+1} - t_i.$$

The value of the constant control u is determined from the slope of the switching function at the switch time t_i. That is,

$$u = u_{max} \quad \text{if} \quad \dot{f}_s(t_i) < 0$$

or

$$= 0 \quad \text{if} \quad \dot{f}_s(t_i) > 0. \quad (9.58)$$

The recurrence equations for the performance index $J(t) = \int_0^t u(t)dt$ is similarly obtained to be

$$J(t_{i+1}) = J(t_i) + u(t_{i+1} - t_i) \tag{9.59}$$

where u is given by equation (9.58). Equations (9.57) through (9.59) are then used to integrate from t_1 to t_{n+2} where $t_1 = 0$; t_i, $i = 2, n + 1$ are then n switch times; and $t_{n+2} = T$. In order to determine the proper control (u) at t_1 we set $\dot{f}_s(t_1) = - \dot{f}_s(t_2)$.

The integration of the costate equation is obtainable in closed form as shown in equations (8.23). Thus, from equations (8.23) and (9.57) through (9.59) we can obtain all the numerical quantities necessary to calculate $\bar{J}(p_0)$ and $\partial\bar{J}(p_0)/\partial p_0$.

D. Digital Computer Program

All of the aforementioned logic and subroutines have been combined into a single digital computer program entitled "THESIS" which solves the subject problem. This program is written in FORTRAN IV for the CDC-6600 digital computer and is available upon request. A functional flow diagram of this program is shown in figure 9.7. The program is overlaid into two links. The first link computes the solution and writes the printed output and a plot tape (if requested); the second link reads the plot tape and plots the requested data with the Calcomp plotter.

In the MAIN (Link 1) program, FLEPOW is called to find p_0^*, the minimizing value of $- \bar{J}(p_0)$. FLEPOW then repeatedly calls FCNGRAD

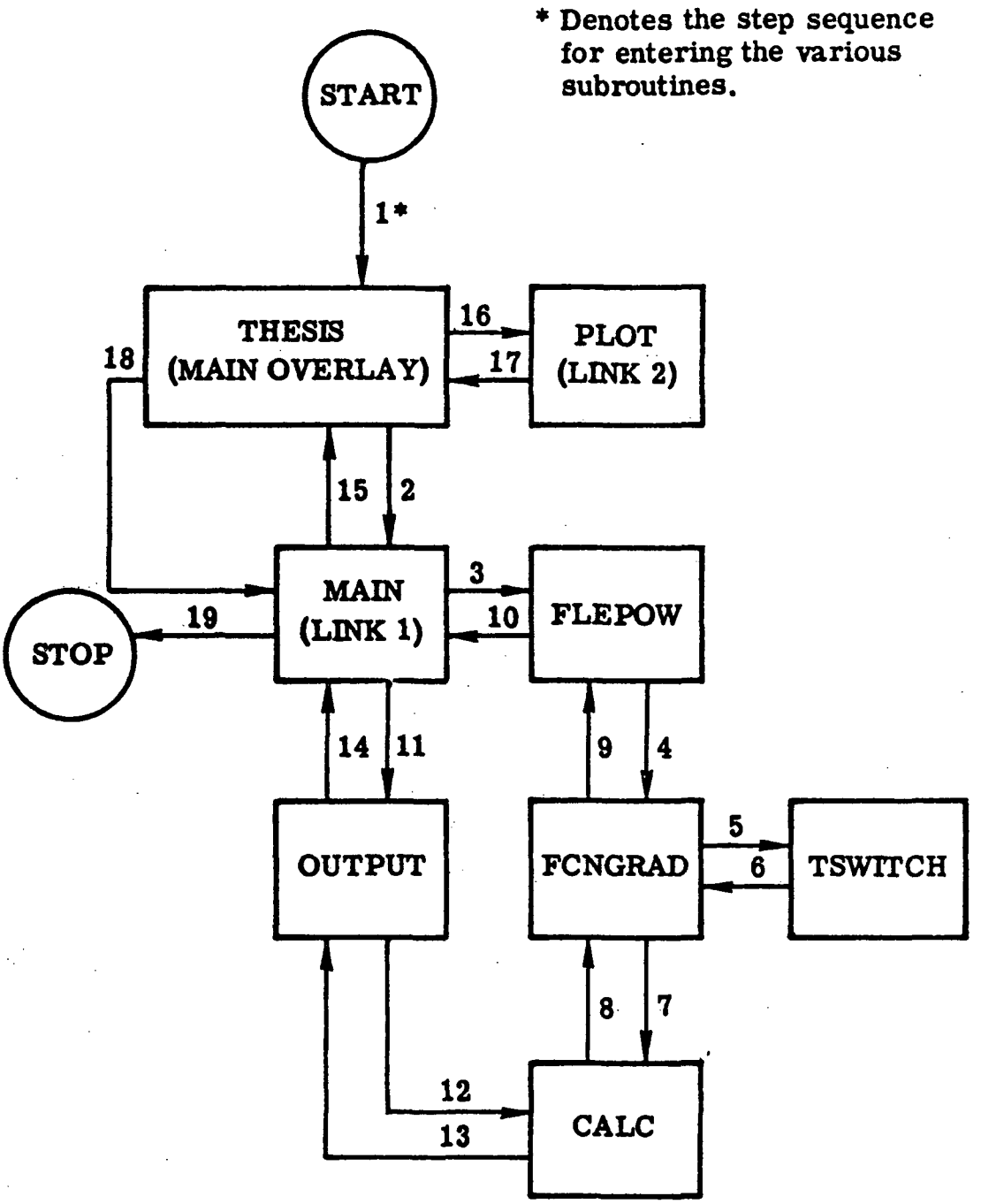

Figure 9.7.- Flow diagram for digital computer program.

until the solution is converged. FCNGRAD in turn calls TSWITCH and CALC. After converging on the solution (p_0^*) FLEPOW returns to MAIN which then calls for the OUTPUT. OUTPUT again repeatedly calls CALC which integrates the state equations and the performance index over subdivisions of the switch time intervals ($t_{i+1} - t_i$)as necessary to define a smooth continuous curve for the printed and plotted output.

The development of the described computer program completes the primary objective of this paper, which is to solve the stated control problem. The remaining task is to investigate the basic nature of the solutions.

X. THE EFFECTS OF SYSTEM PARAMETERS ON THE OPTIMAL CONTROL

It has been shown in reference 22 that the ideal fuel-optimal control is impulsive. In this chapter we shall first look at the ideal impulsive controls in order to gain an insight into the optimal control solutions to the subject problems. We shall then look at some actual solutions for typical classes of initial conditions. Finally, we shall discuss the combined effect of all the system parameters on the fuel consumption.

A. Impulsive Fuel-Optimal Controls

Let us assume that the nondimensional control variable, u, is impulsive and of the form

$$u = \mu\, \delta(t - t_1) \tag{10.1}$$

where δ is the Dirac delta function and μ is the magnitude. The integration of the first two equations of (7.25) using equation (10.1) then yields

$$x_1(t_1) = x_1(0) - \mu \sin t_1$$

and (10.2)

$$x_2(t_1) = x_2(0) - \mu \cos t_1.$$

Since x_1 and x_2 are the components of the angular momentum vector, h, we then have from equations (10.2)

$$\Delta h = \sqrt{\Delta x_1^2 + \Delta x_2^2} = \mu \tag{10.3}$$

where $|\Delta h| = |h(t_1) - h(0)|$ and $\Delta x_i = [x_i(t_1) - x_i(0)]$, $i = 1, 2$. An illustration of the trajectory of the vehicle in the $\psi - \theta$ plane due to this impulse is given in figure 10.1. Starting at $t = 0$ from the point (ψ_0, θ_0), the trajectory is a circle with the center at h_0 and the radius ρ_0. At time $t = t_1$ the impulsive torque produces a step shift μ in the momentum vector from h_0 to h_1. Then for $t > t_1+$, the motion is another circle with the center at h_1 and a radius of ρ_1. The direction of the angular momentum shift is in the direction of the torque vector at $t = t_1$. The torque vector spins with the body and thus movement can be achieved in any desired direction by proper phasing of the impulse.

1. Two-Impulse Fuel-Optimal Control - It is clear that the results derived for a single impulse can be extrapolated to any number of impulses. This procedure was used in reference 22 to graphically show that for unlimited control magnitude and orientation, the trajectory in the ψ-θ plane can always be driven to the origin with minimum-fuel two-impulse control scheme. The two-impulse control laws fall into two classes: (1) the initial nutation circle excludes the origin and (2) the initial nutation circle includes the origin.

An illustration of the "class 1" control law is given on figure 10.2. From any initial nutation circle and any initial point α_0 on it, the first impulse (μ_1) must shift h_0 to h_1 located at the intersection of the perpendicular bisector of $O\alpha_0$ and Oh_0. The following trajectory then passes through the origin, O. When O is reached, the second

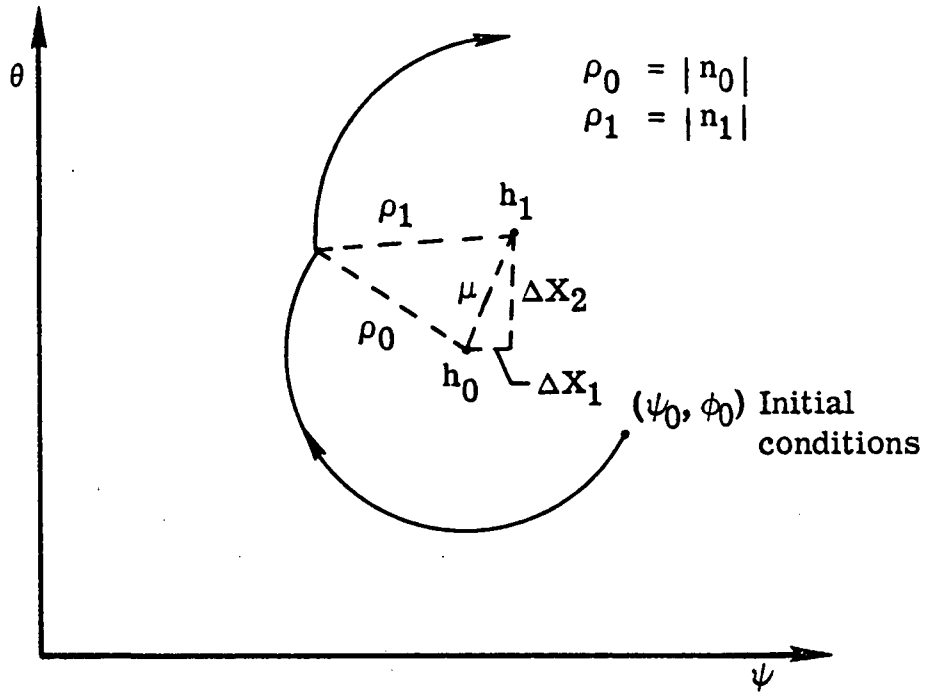

Figure 10.1.- Trajectory in the ψ-θ plane resulting from impulsive control.

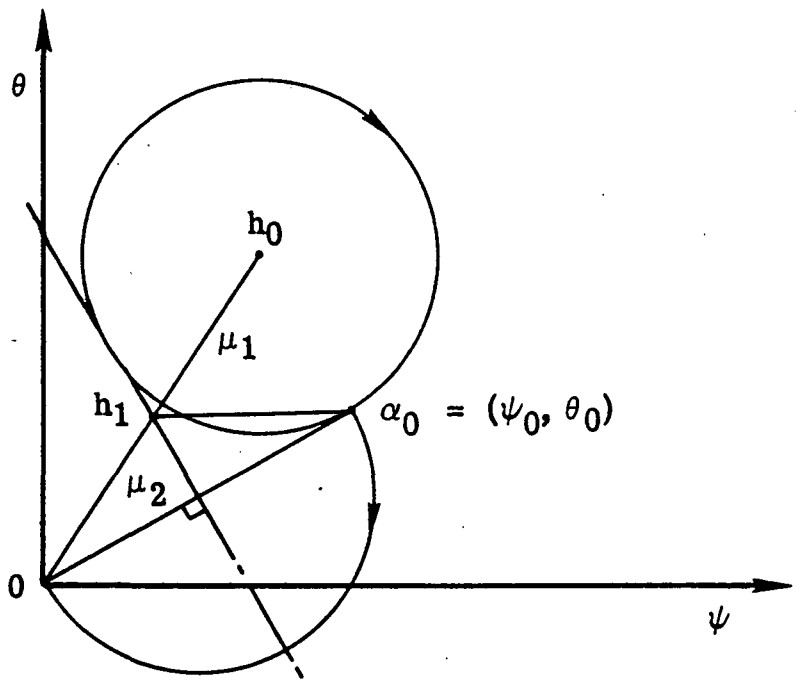

Figure 10.2.- Class 1 fuel-optimal two-impulse control.

impulse (μ_2) shifts h_1 to 0, which aligns the momentum vector with the origin and reduces the radius of the nutation circle to zero. The total fuel consumption

$$\mu_1 + \mu_2 = |h_0| \tag{10.4}$$

is clearly the minimum value for moving h_0 to 0. The time for the control is proportional to the arc length $0\alpha_0$.

An illustration of the "class 2" control law is given in figure 10.3. The first impulse (μ_1) decreases the radius (ρ_0) so that the trajectory again passes through the origin. The second impulse μ_2 then shifts h_1 to the origin as the trajectory reaches 0. The total fuel consumed is

$$\mu_1 + \mu_2 = \rho_0 = |n_0| \tag{10.5}$$

and again is clearly the minimum. The minimum fuel bounds given by equations (10.4) and (10.5) are seen to be identical to those of equations (8.52) and (8.53) and provide us with a physical explanation.

2. Approximations to Impulsive Controls - In practice impulsive torque must be approximated by firing a reaction jet through a sector of the vehicle spin cycle centered about the desired direction of impulse. This results in a cosine loss as indicated in figure 10.4. The efficiency, E, in converting fuel consumption into useful impulse can be derived from figure 10.4 as

"Page missing from available version"

$$\%E = \frac{2\int_0^{\gamma_1} u_{max} \cos\gamma \, d\gamma}{2\, u_{max}\, \gamma_1} \times 100$$

$$= \frac{\sin\gamma_1}{\gamma_1} \times 100 \qquad (10.6)$$

A tabulation of E versus γ_1, the firing sector half-angle, is given in table 10.1. It is seen that the maximum efficiency is obtained when the firing sector approaches zero.

From the foregoing discussions, we would intuitively expect the actual solutions to the subject problem of this paper to be a series of short pulses which approximate, in some fashion, the fuel-optimal two-impulse control. It is also intuitive that this approximation would be the closest for a final time greater than the impulsive minimum time and the nutation rate $r \to 0$.

B. Typical Solutions for Various Classes of Initial Conditions

For the purposes of discussing the actual fuel-optimal control we shall expand the previous classes of initial conditions to the following:

Class 1 - the initial nutation circle excludes the origin.

Class 2 - the initial nutation circle includes the origin.

Class 3 - the initial nutation is zero.

Class 4 - the initial angular momentum is zero.

It is seen that classes 3 and 4 are really just degenerate subsets of the general classes 1 and 2, respectively. All possible sets of

TABLE 10.1.- IMPULSIVE EFFICIENCY AS A FUNCTION OF THE FIRING SECTOR HALF-ANGLES

Firing sector half angle, deg.	Percent impulse efficiency
0.0	100%
5.0	99.92
10.0	99.47
12.5	99.19
15.0	98.85
20.0	97.98
25.0	96.85
30.0	95.49
40.0	92.07
50.0	87.77
60.0	82.75
70.0	76.91
80.0	70.53
90.0	63.66

initial conditions are then included in these four classes. It is beyond the scope of this paper to present an exhaustive parameter study of various initial conditions. Instead, we shall present a typical solution for each of the four classes of initial conditions for a slender rod ($r = 0.1$) and for a thin disk ($r = 1.9$). These eight cases are then representative of the form of the optimal control for a very wide range of conditions. The input values for the initial conditions and the other system parameters are given in table 10.2. The corresponding computed fuel consumption along with the parameter values for the switching function are given in table 10.3. Also, curves of the switching functions versus time, and θ versus ψ (for each of the eight cases in tables 2 and 3) are given in figures 10.5 through 10.12, respectively. On the ψ-θ plots, the incremental steps in the angular momentum are shown by the circles. The total number of firings is then one less than the total number of circles.

One of the most important things to notice from figures 10.5(a) through 10.12(a) and from table 10.3 is that the switching functions and the minimum fuel for cases 1 through 4 ($r = 0.1$) are (for all practical purposes) identical to cases 5 through 8, respectively. In fact, it has been found that in all cases, the control for an inertia ratio of r (where $r < 1$) is identical to an inertia ratio of $(2 - r)$. Also, by comparing figures 10.5(b) through 10.8(b) with figures 10.9(b) through 10.12(b), respectively, it is seen that the motion of the angular momentum is identical even though the nutation motion is grossly different. From the comments following equation (8.33), one might have

TABLE 10.2.- DIMENSIONLESS INPUT PARAMETER VALUES

FOR TYPICAL SOLUTIONS

Case	r	T	u_{max}	x_{10}	x_{20}	x_{30}	x_{40}	Class
1	.1	95	.1	.4	0	0	.6	1
2	.1			.1	0	0	.2	2
3	.1			.4	0	0	0	3
4	.1			0	0	0	.2	4
5	1.9			.4	0	0	.2	1
6	1.9			.1	0	0	.2	2
7	1.9			.4	0	0	0	3
8	1.9	95	.1	0	0	0	.2	4

TABLE 10.3.- COMPUTED PARAMETER VALUES FOR TYPICAL SOLUTIONS

Case	A_1	β_1, deg.	A_2	β_2, deg	J(u*)
1	1.021	.1056	.0506	-94.74	.4061
2	.0128	-5.162	1.004	-89.96	.2007
3	1.012	0	.0092	-99.00	.4016
4	.0020	-10.00	1.003	-90.0	.2001
5	1.021	.1056	.0506	-85.26	.4061
6	.0128	-5.162	1.004	-90.04	.2007
7	1.012	0	.009	-81.00	.4016
8	.0020	-10.00	1.003	-90.00	.2001

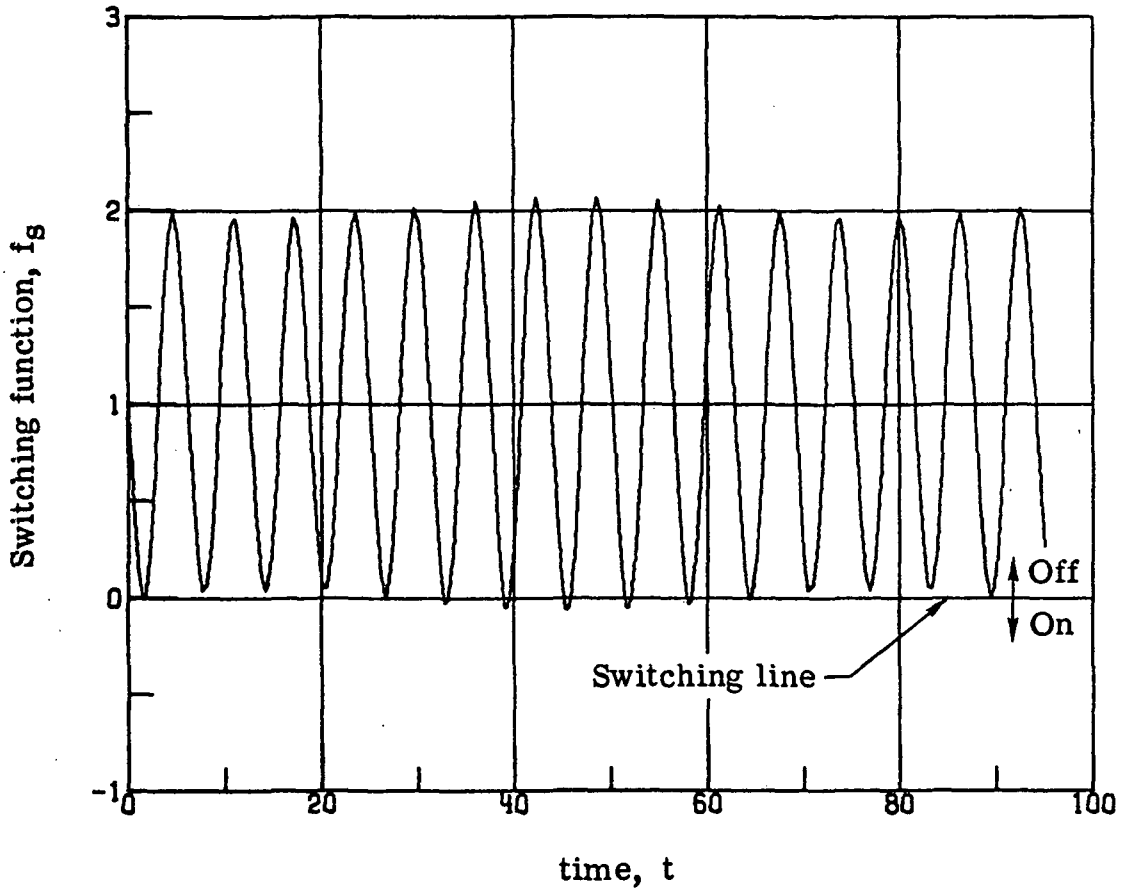

(a) Switching function versus time

Figure 10.5.- Solutions for class 1 initial conditions (case 1, r = 0.1).

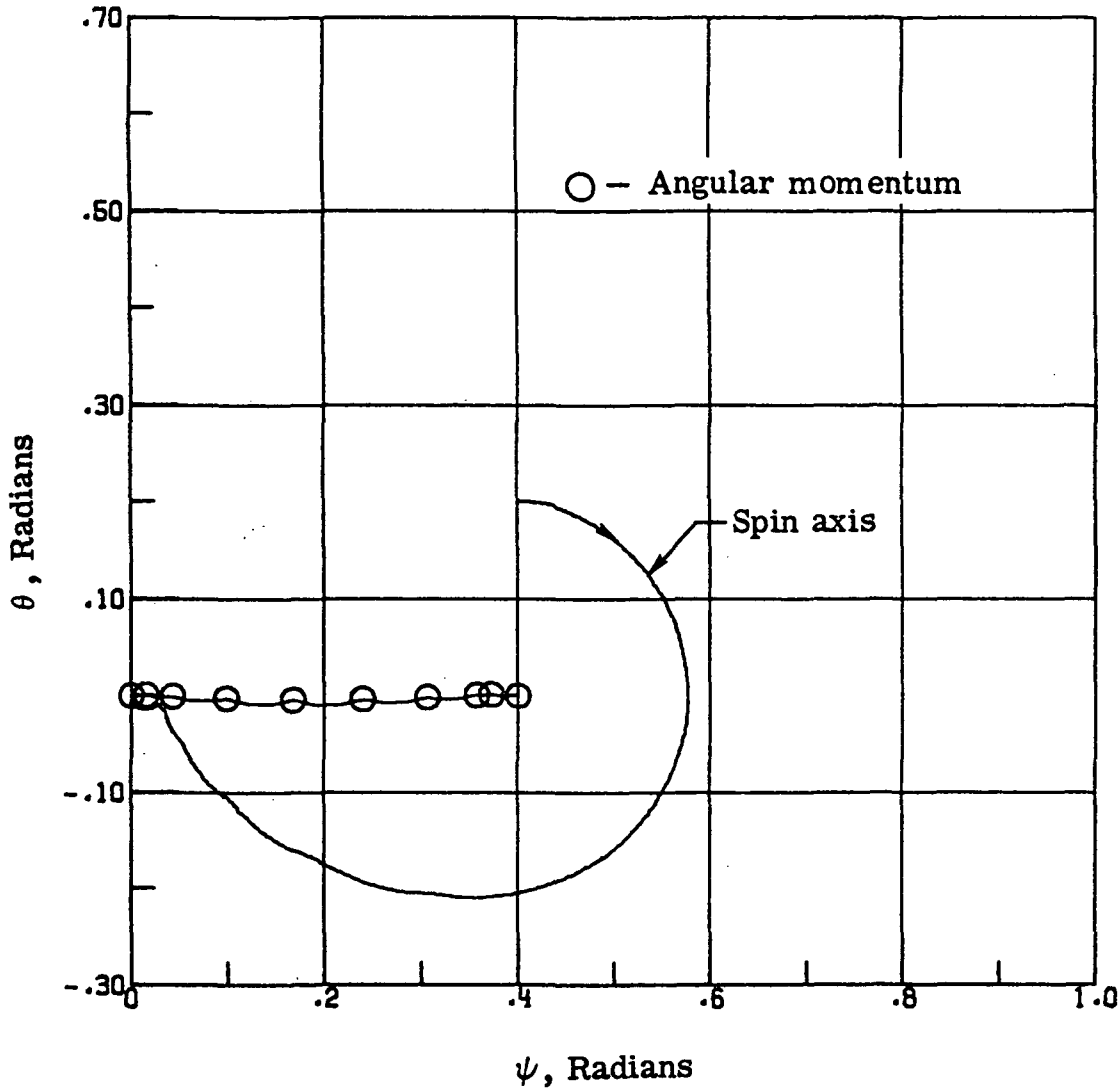

(b) Pitch angle versus yaw angle

Figure 10-5.- Concluded.

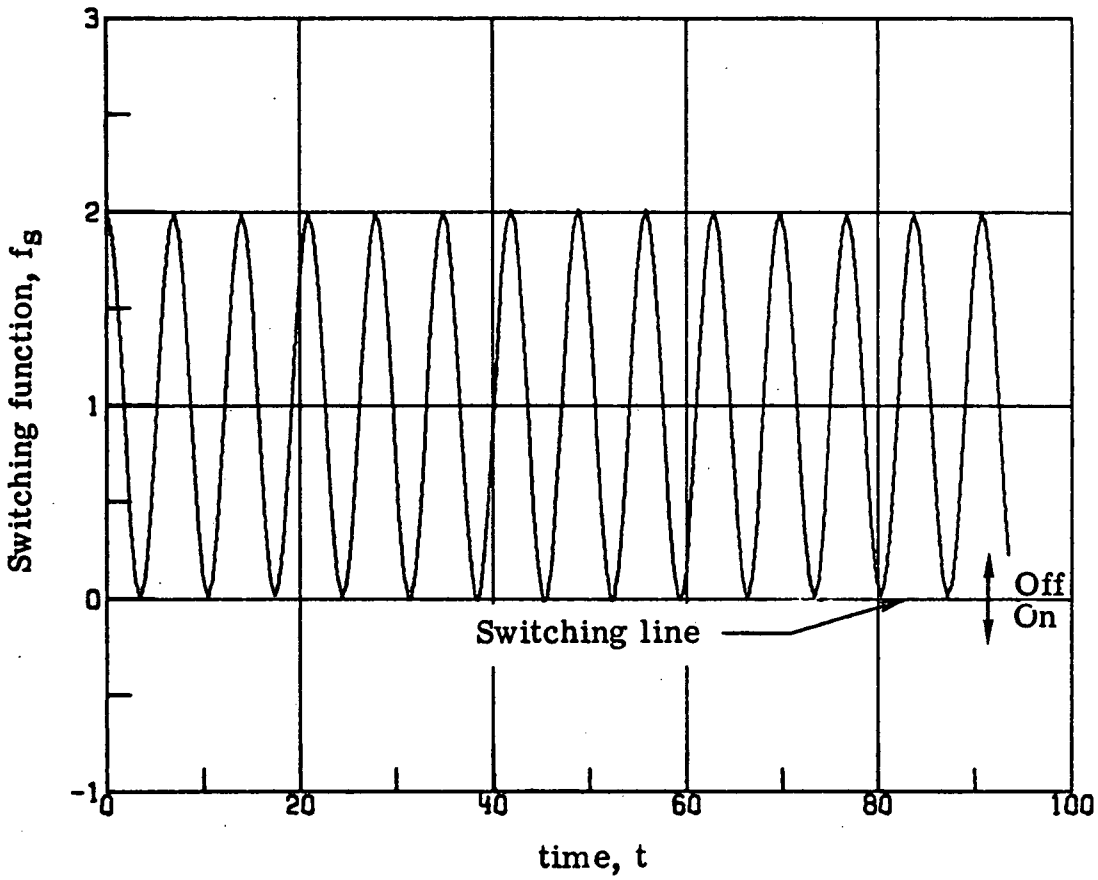

(a) Switching function versus time

Figure 10.6.- Solutions for class 2 initial conditions (case 2, r = 0.1).

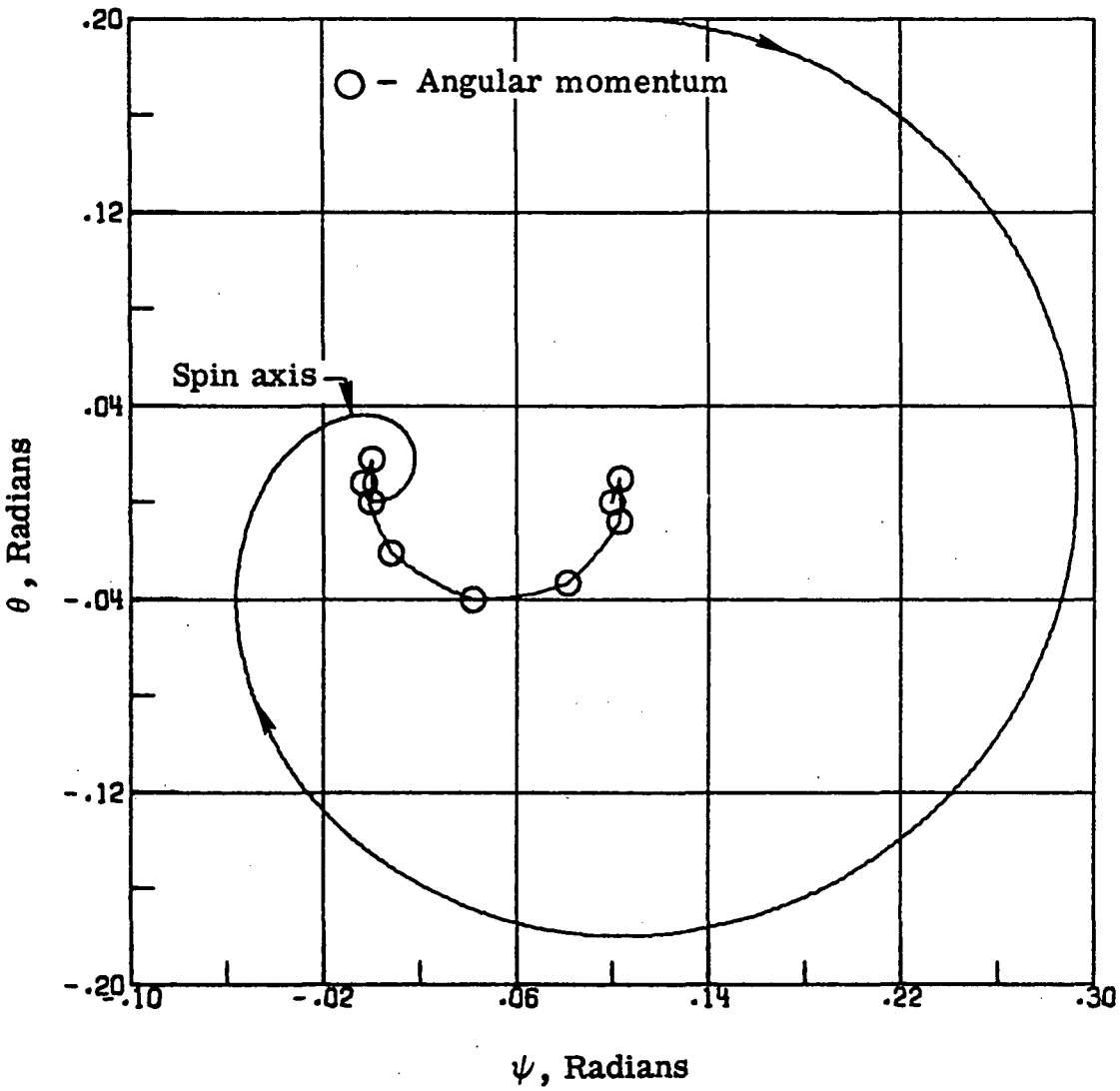

(b) Pitch angle versus yaw angle

Figure 10-6.- Concluded.

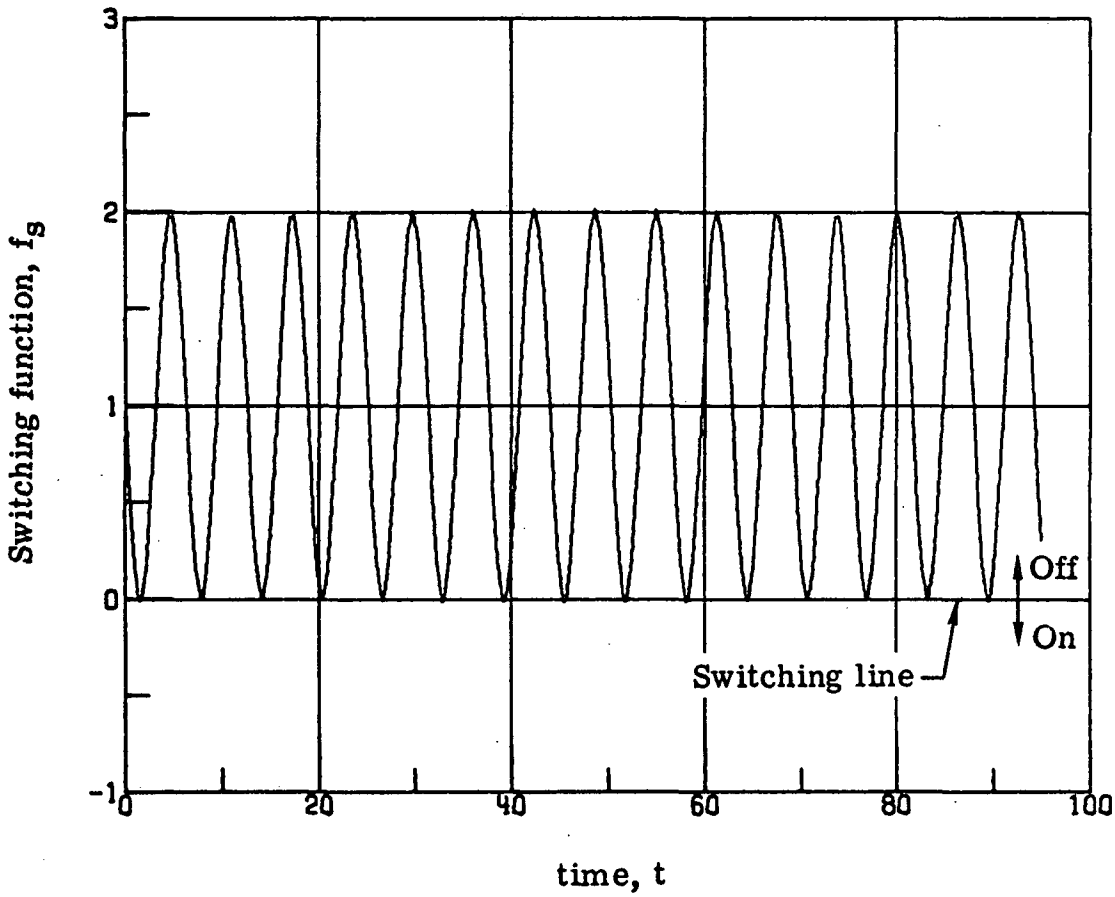

(a) Switching function versus time

Figure 10.7.- Solutions for class 3 initial conditions (case 3, r = 0.1).

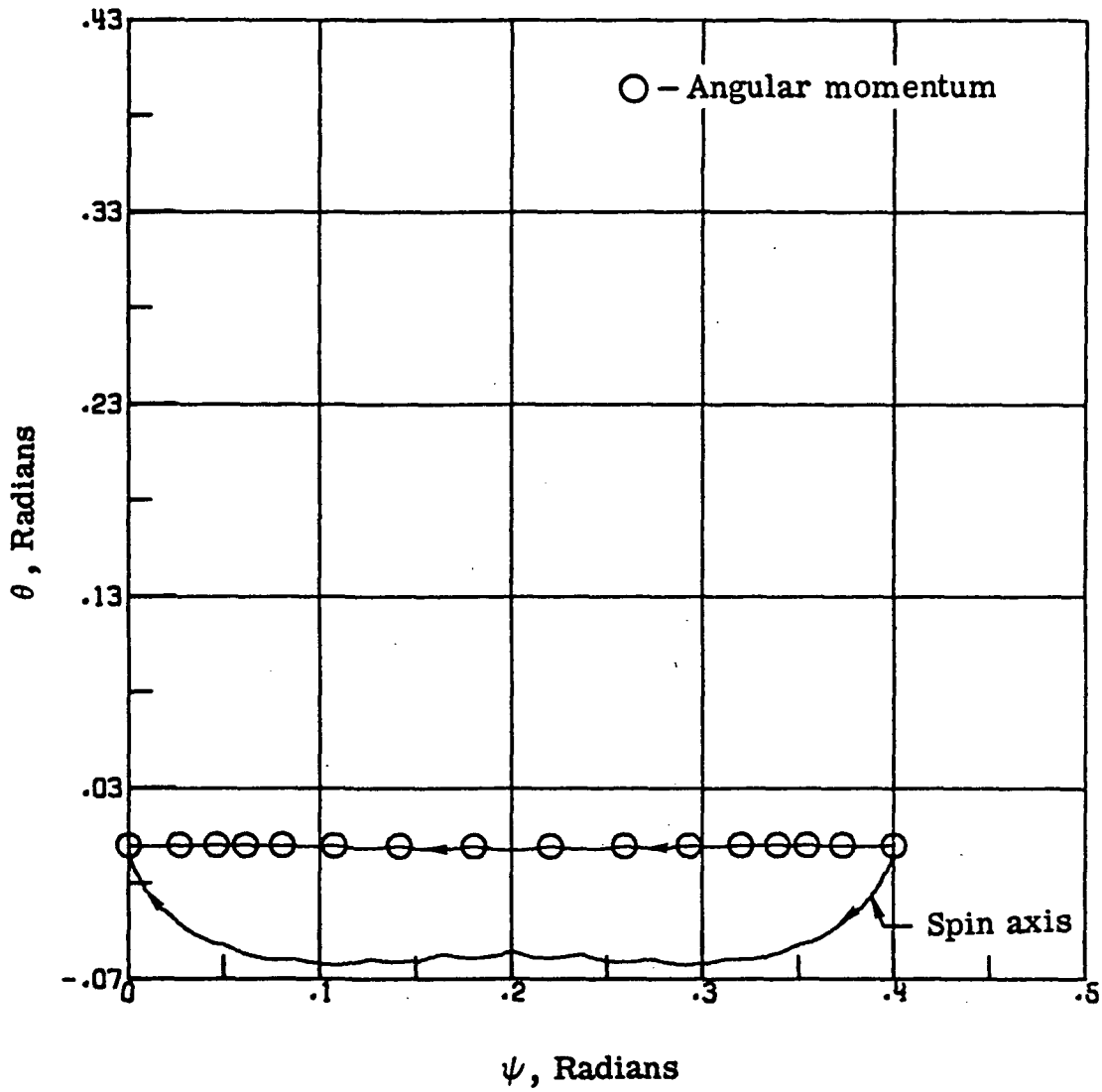

(b) Pitch angle versus yaw angle

Figure 10-7.- Concluded.

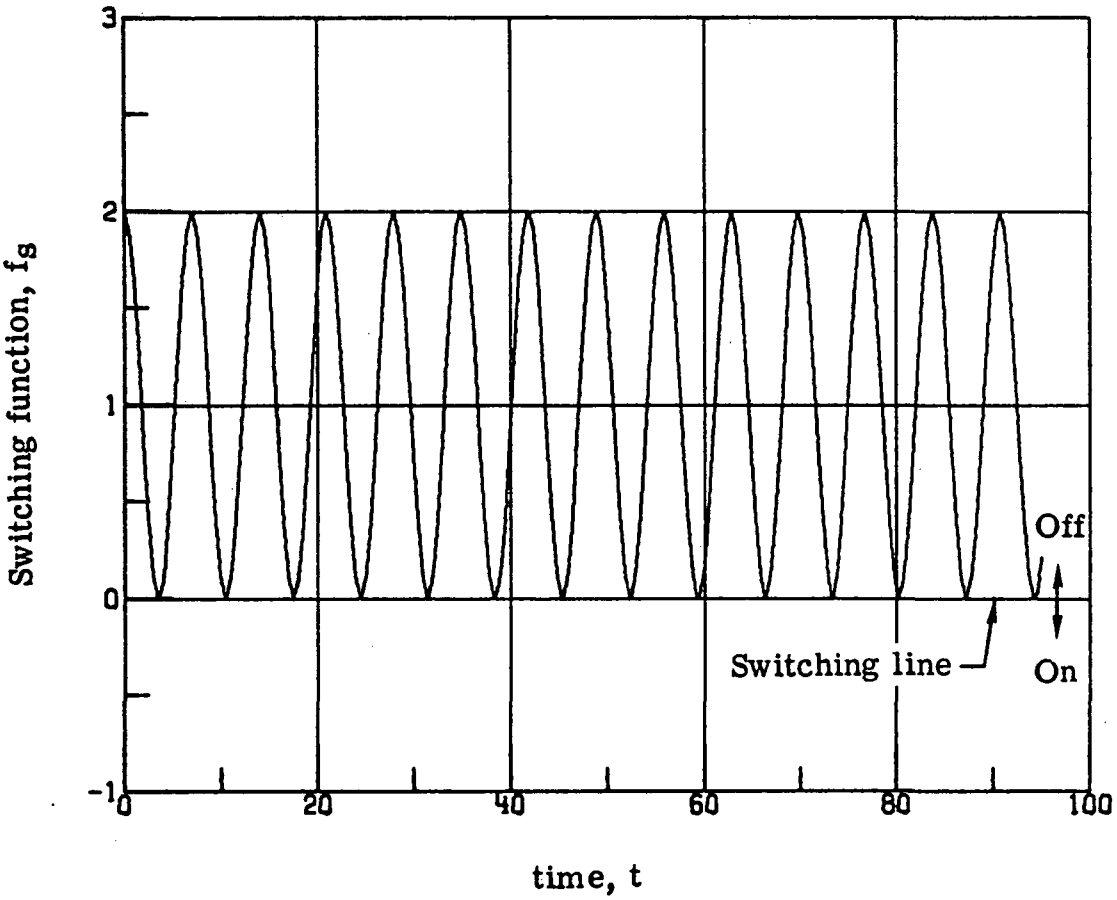

(a) Switching function versus time

Figure 10.8.- Solutions for class 4 initial conditions (case 4, r = 0.1).

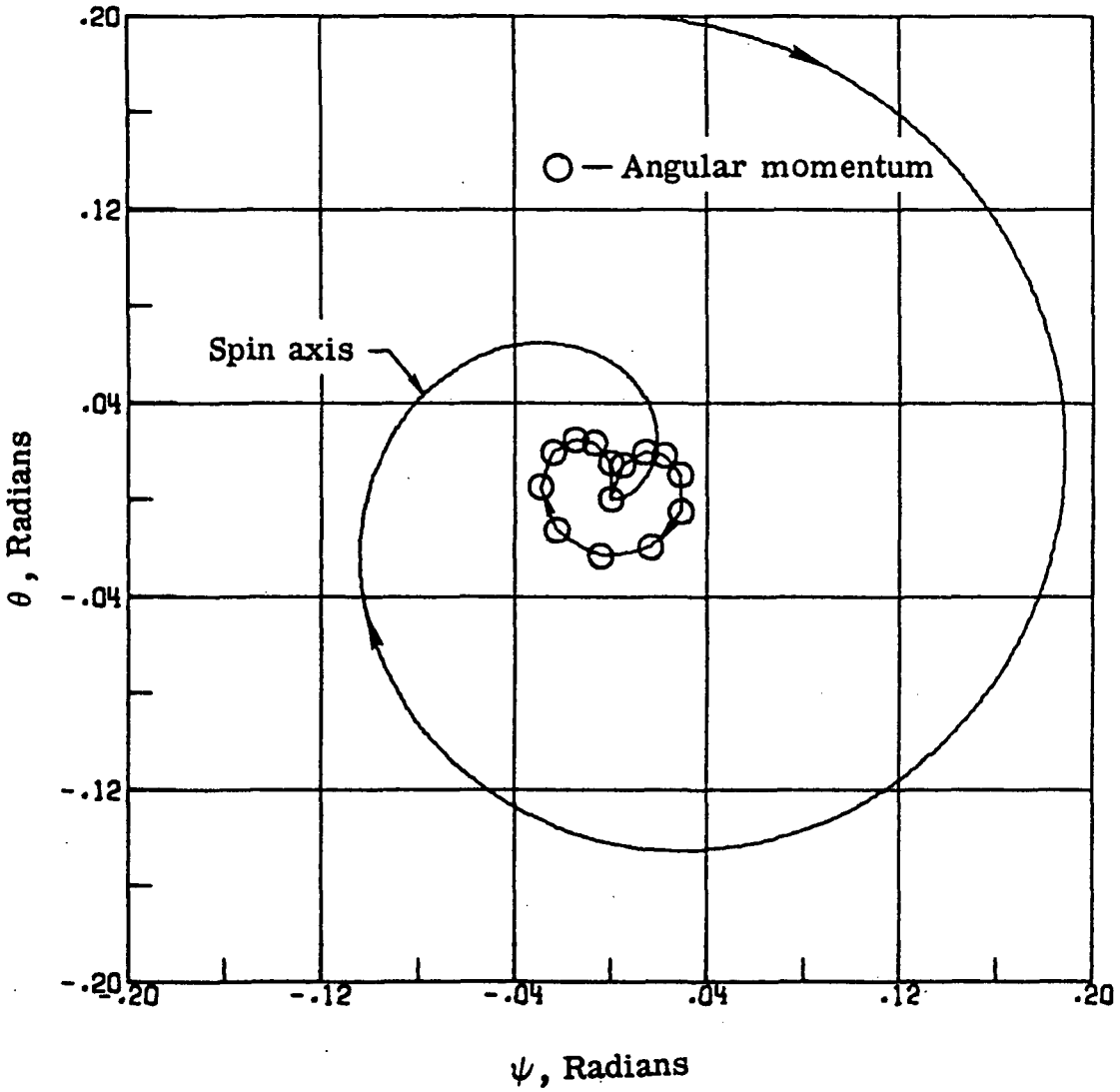

(b) Pitch angle versus yaw angle

Figure 10-8.- Concluded.

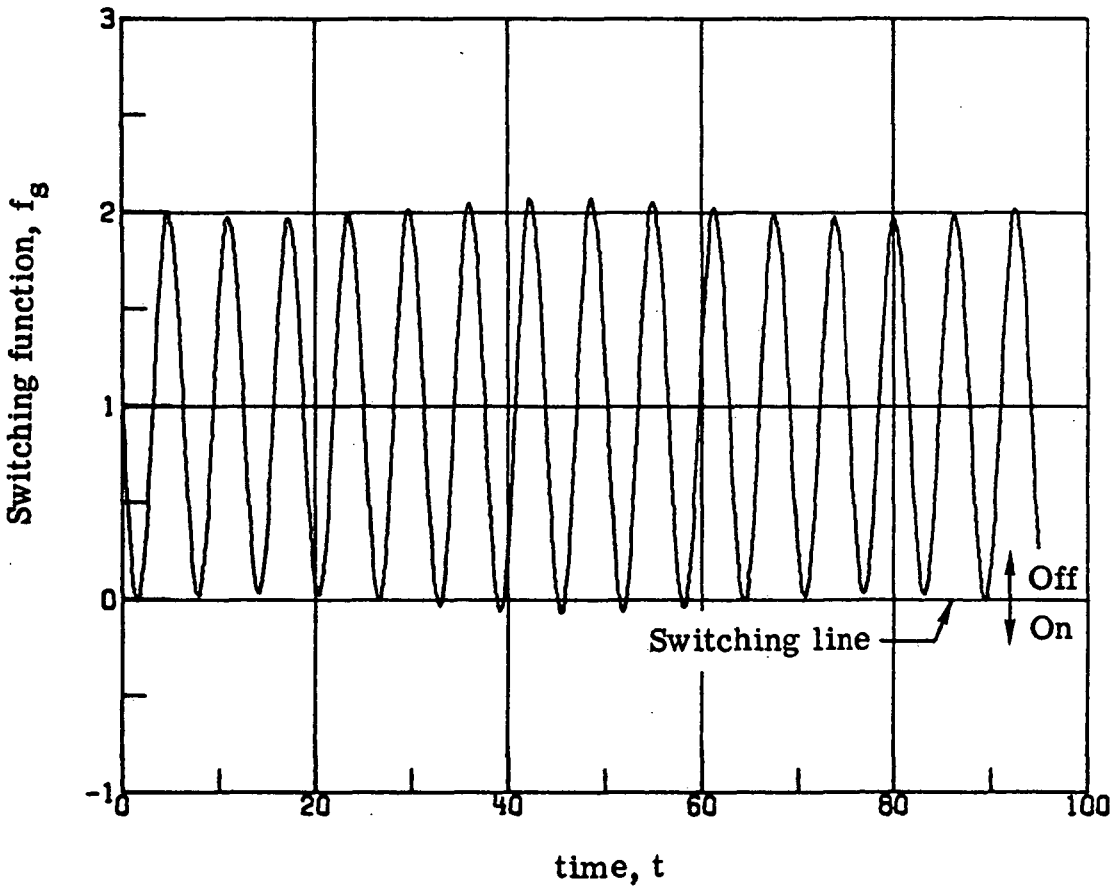

(a) Switching function versus time

Figure 10.9.- Solutions for class 1 initial conditions (case 5, r = 1.9).

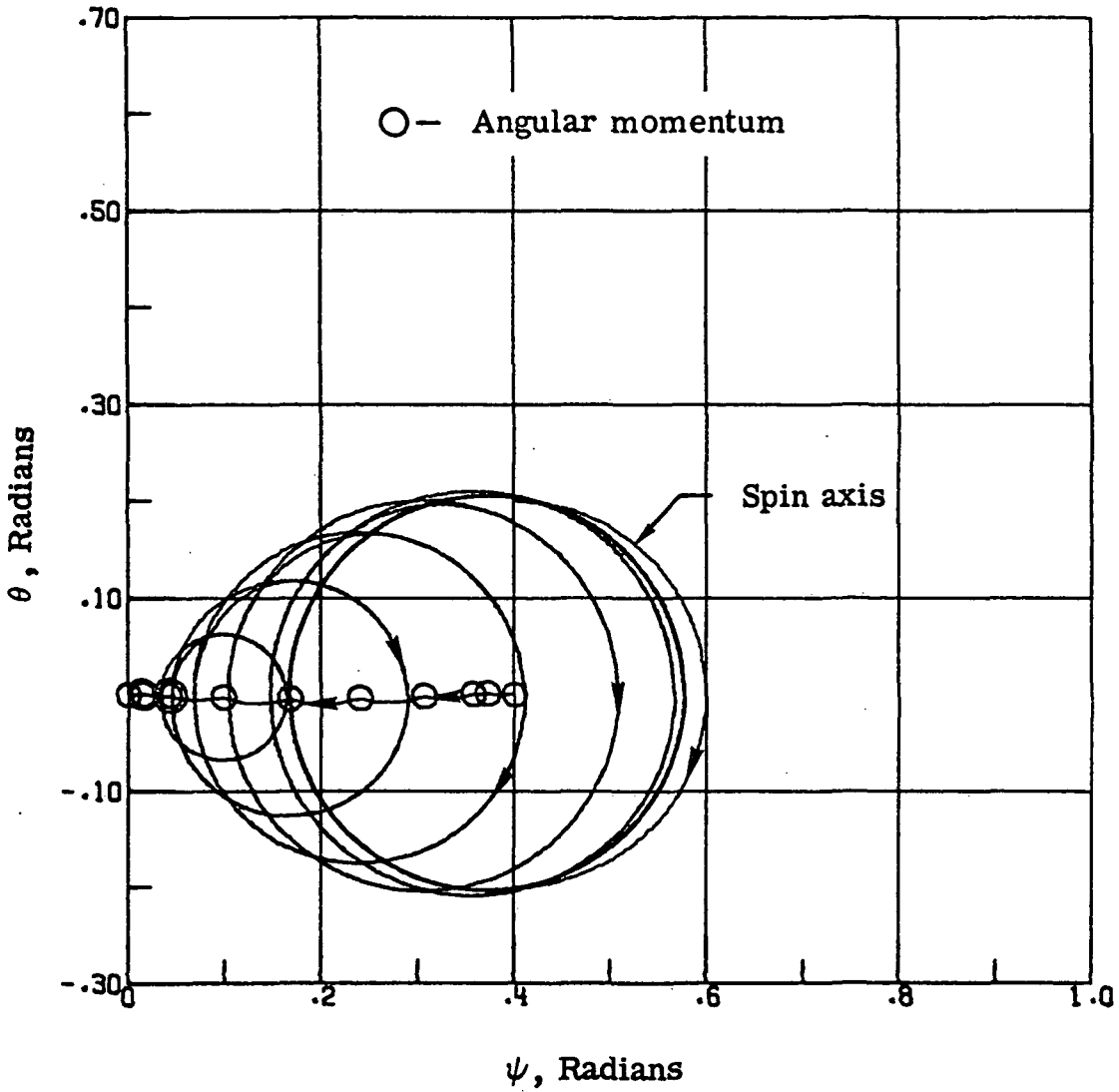

(b) Pitch angle versus yaw angle

Figure 10-9.- Concluded.

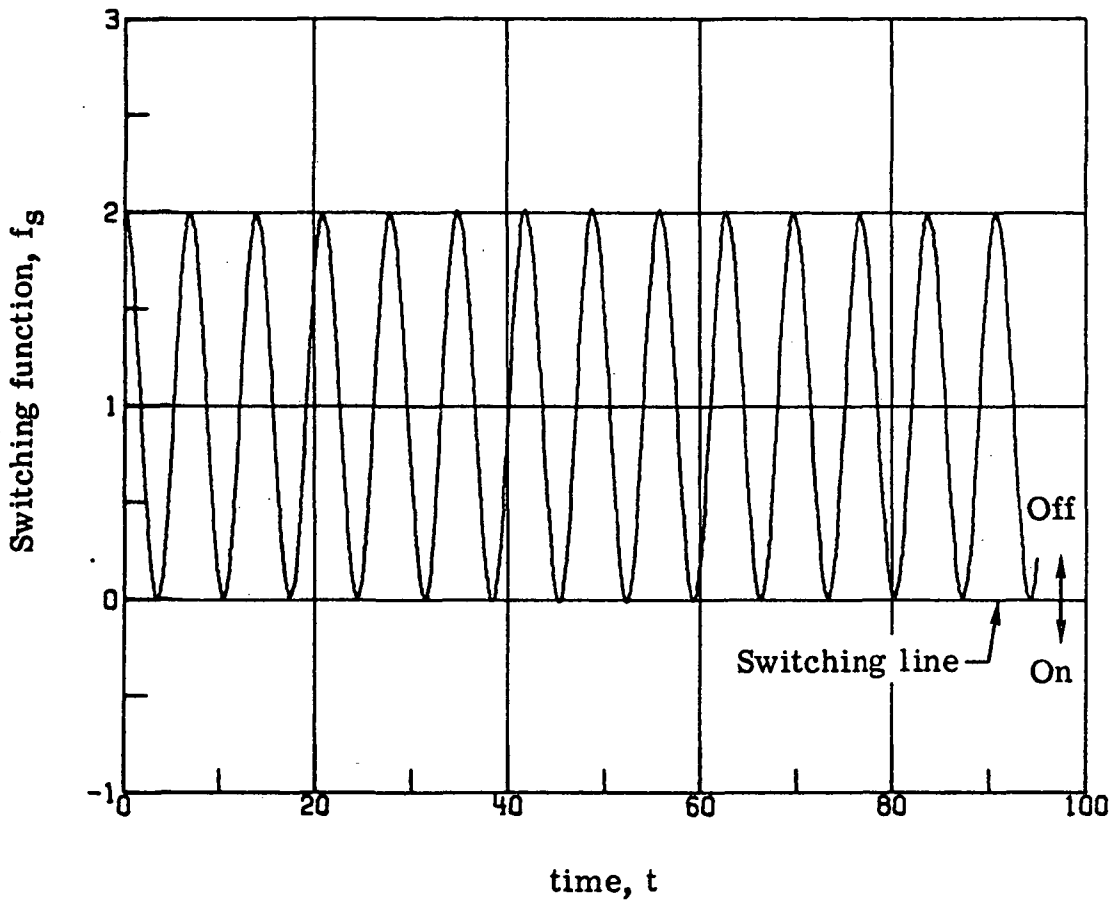

(a) Switching function versus time

Figure 10.10.- Solutions for class 2 initial conditions (case 6, r = 1.9).

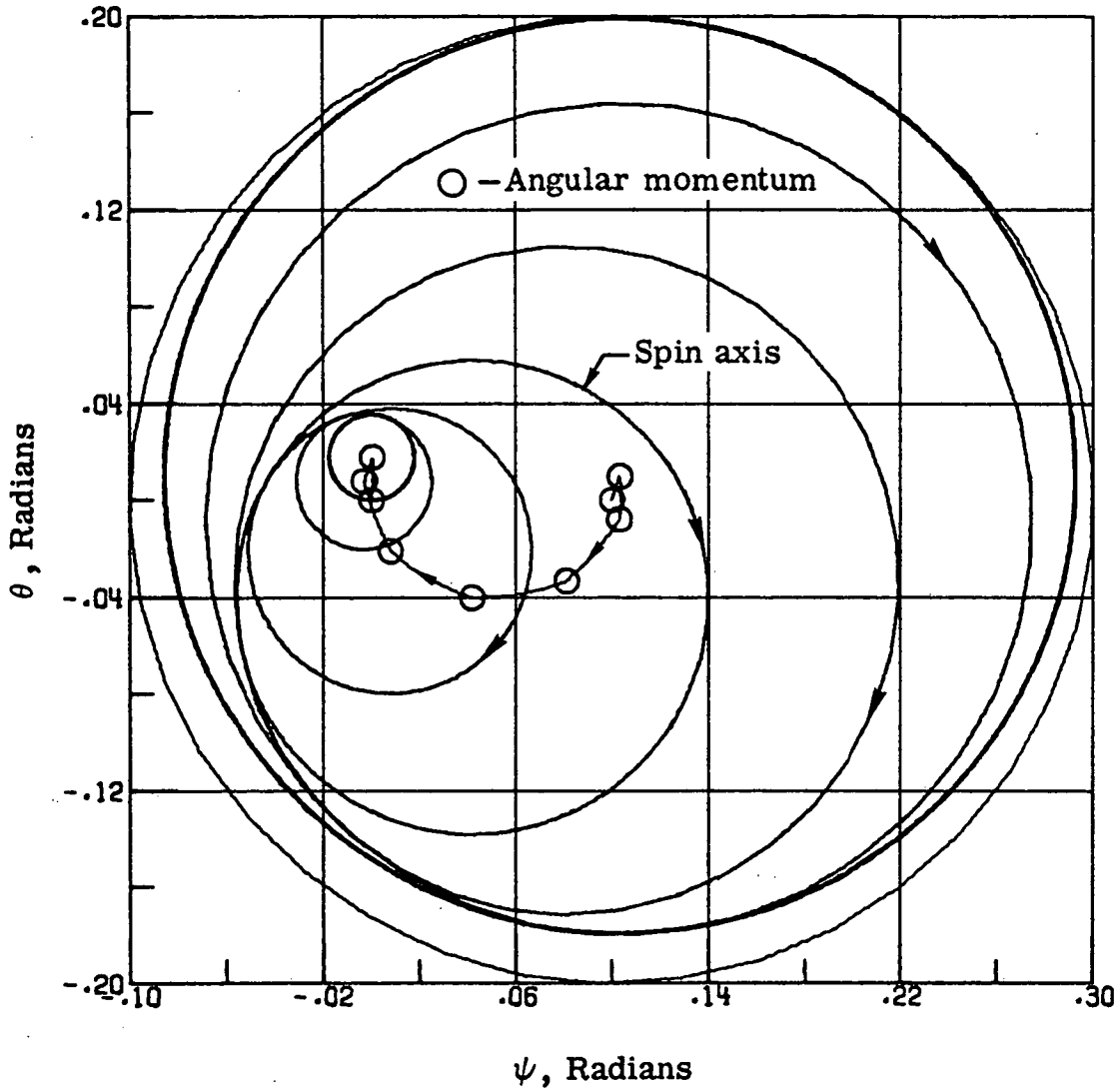

(b) Pitch angle versus yaw angle

Figure 10-10.- Concluded.

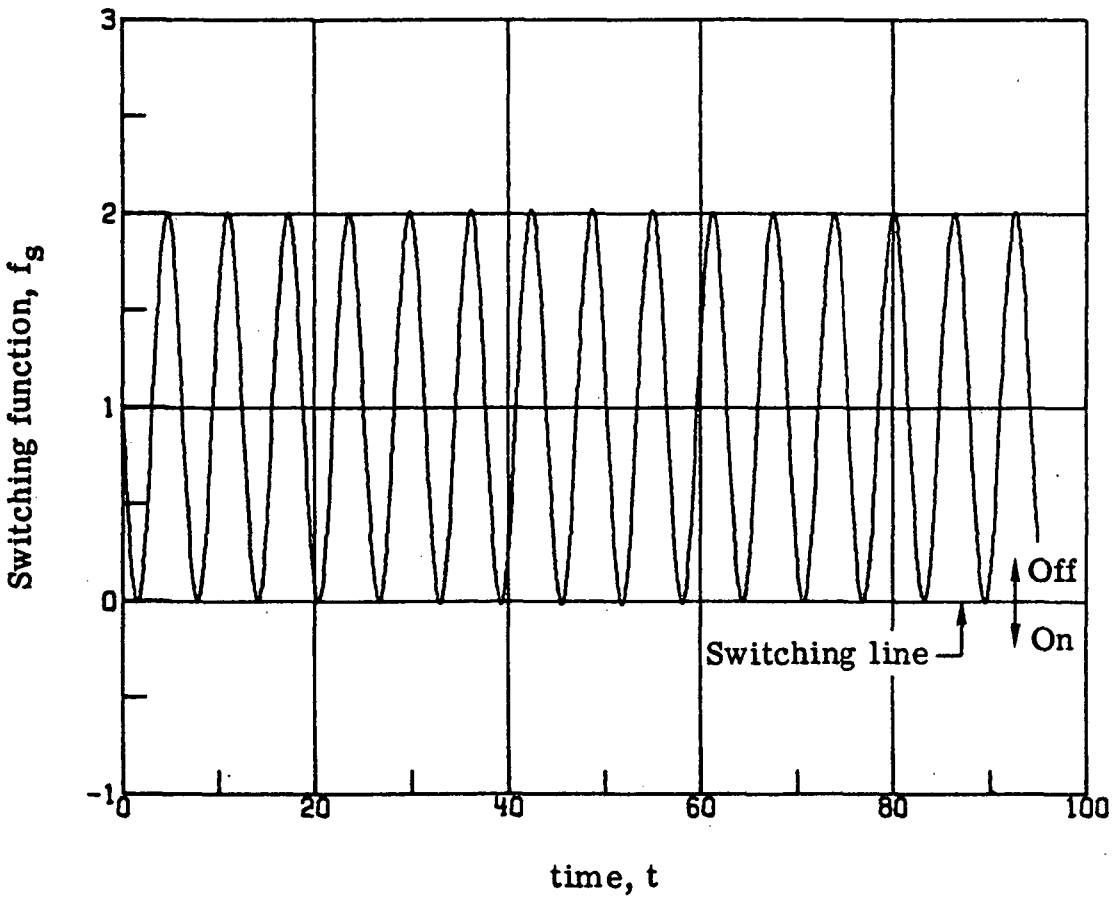

(a) Switching function versus time

Figure 10.11.- Solutions for class 3 initial conditions (case 7, r = 1.9).

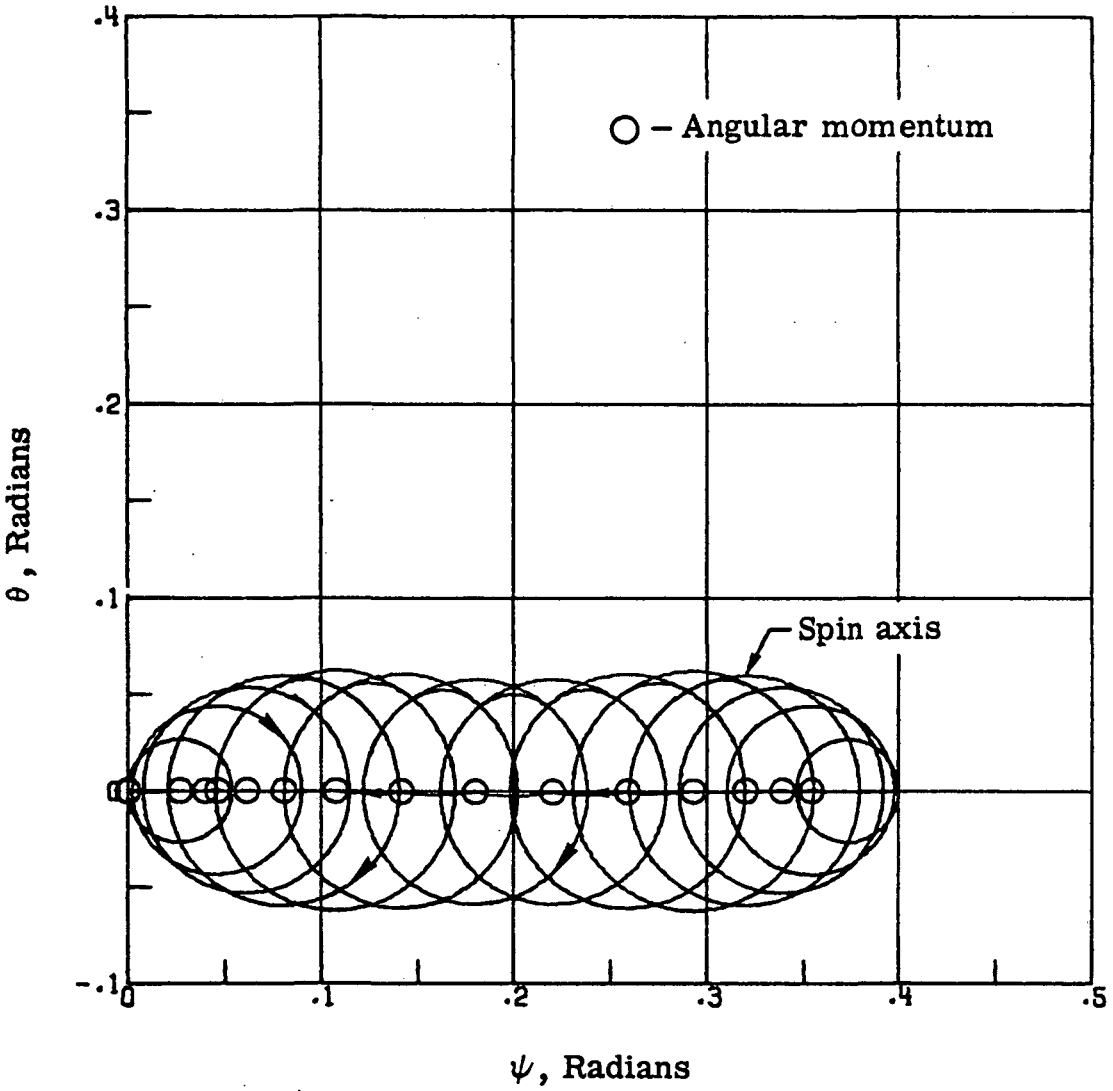

(b) Pitch angle versus yaw angle

Figure 10-11.- Concluded.

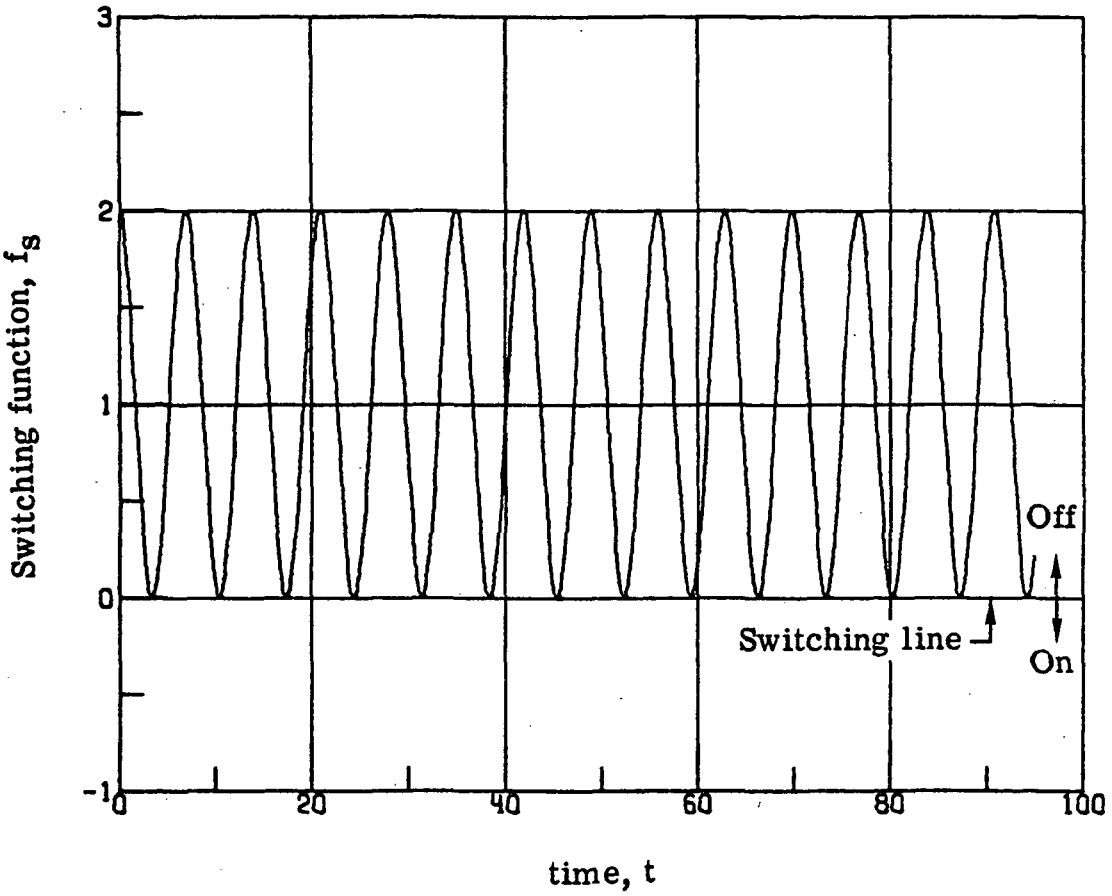

(a) Switching function versus time

Figure 10.12.- Solutions for class 4 initial conditions (case 8, r = 1.9).

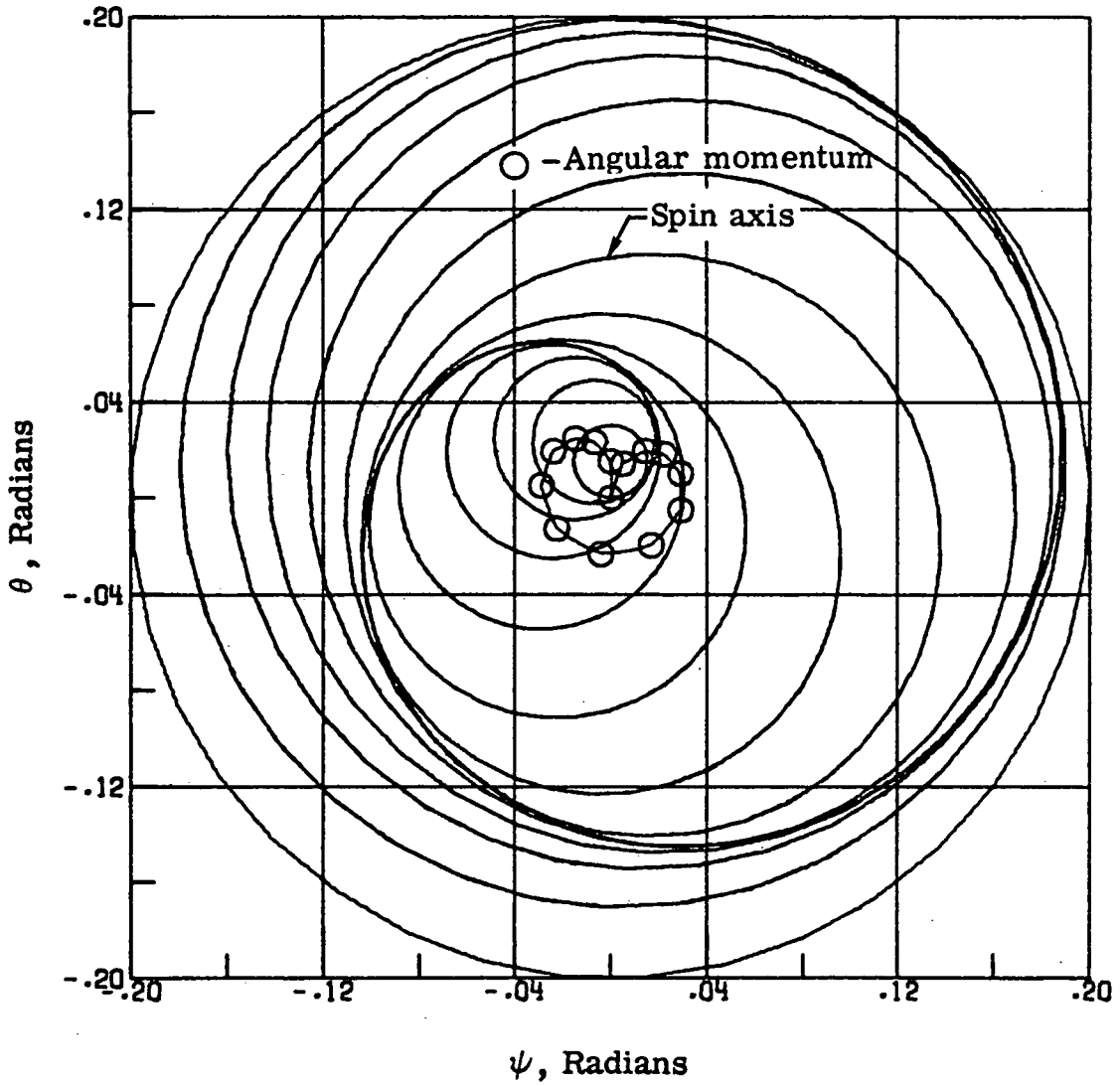

(b) Pitch angle versus yaw angle

Figure 10-12.- Concluded

anticipated these results. In view of this phenomena, the discussion for the remainder of the paper will primarily be limited to values of $r < 1$ since the motions for this condition are easier to intuitively understand.

For cases 1 and 3 the impulsive minimum fuel is $|h_0| = 0.4$ and for cases 2 and 4 it is $|n_0| = 0.2$. Comparing these values with those of table 10.3, we note that the actual fuel consumption is almost identical to the impulsive values. Another indication of this efficiency for cases (1) and (3) is seen from figures 10.5(b) and 10.7(b) by the nearly straight line movement of the angular momentum to the origin. This straight line motion also indicates that the phasing of the pulse remains nearly constant and always occurs at the same point in each spin cycle. In contrast, we note from cases 2 and 4 (figs. 10.6(b) and 10.8(b)) that the angular momentum moves in an arc, which indicates a time varying phasing of the pulse in each spin cycle. The main resemblance between the actual and impulsive fuel-optimal controls is that for class 1 and 3 initial conditions, the angular momentum tends to move in a straight line and for class 2 and 4 initial conditions, it does not.

Another interesting facet to note from figures 10.7 and 10.8 is that for the class 3 and 4 initial conditions, the amplitude modulation of the switching function approaches zero and one firing is obtained every spin cycle. For the class 1 and 2 initial conditions of figures 10.5 and 10.6 there is amplitude modulation of the switching functions which causes firings to be skipped for several spin cycles.

C. The Effect of the System Parameters on Minimum Fuel Consumption

From all of the foregoing discussion in this section we might gather that the minimum fuel consumption is a complex function of the initial conditions, the control magnitude u_{max}, the inertia ratio r, and the final time T. Some idea of the nature of this function can be obtained by analyzing the results we have obtained. First, we have shown that for an efficient control, the total impulse is equal to

$$J_{min} = \text{maximum of } (|n_0|, |h_0|) \tag{10.7}$$

and secondly, we have shown that the firing sector half angle must be small. Let us assume a firing sector half angle of 20° which is shown in table 10.1 to have an efficiency of approximately 98 percent. The momentum shift per cycle is then (see fig. 10.4)

$$\begin{aligned} \Delta h &= 2\int_0^{\pi/9} u_{max} \cos\gamma \, d\gamma \\ &= 2\, u_{max} \sin\frac{\pi}{9} \approx \frac{2\pi\, u_{max}}{9}. \end{aligned} \tag{10.8}$$

Let us now seek an approximation of the total number of firing cycles which occur. To do this, we look at the task which the optimal control must accomplish, namely

$$\left| \sum_{i=1}^{n} \Delta h_i \right| \approx J_{min} \tag{10.9}$$

and

$$\frac{\sum_{i=1}^{n} \Delta|n_i|}{\left|\sum_{i=1}^{n} \Delta h_i\right|} = \frac{|n_0|}{|h_0|} = \sigma_0 \tag{10.10}$$

where $\Delta h_i = h_{i-1} - h_i$, $\Delta|n_i| = |n_{i-1}| - |n_i|$, h_i and n_i denote the values after the ith firing, and n is the total number of firings. In other words, the magnitude of the vector sum of the momentum impulses must be about equal to J_{min} and the ratio of the sum of the nutation arm changes in magnitude to the magnitude of the vector sum of the momentum changes must be equal to the initial ratio, σ_0, in order to simultaneously reduce both n_0 and h_0 to zero.

To simplify our approximation, let us consider (for the moment) only class 1 and class 3 initial conditions. The typical shift in the angular momentum and nutation arm due to an impulse is then shown in figure 10.13. It is seen that

$$|n_i| = \left\{\left[|n_{i-1}| \sin(\zeta_i - \delta_1)\right]^2 + \left[|n_{i-1}| \cos(\zeta_i - \delta_1) + |\Delta h_i|\right]^2\right\}^{1/2}$$

$$\approx |n_{i-1}| + |\Delta h_i| \cos(\zeta_i - \delta_1) \quad \text{for} \quad \frac{|\Delta h_i|}{|n_{i-1}|} \ll 1$$

or

$$\Delta|n_i| = -|\Delta h_i| \cos(\zeta_i - \delta_1) \tag{10.11}$$

where $\delta_1 = \tan^{-1}(x_{20}/x_{10})$ and ζ_i is the mean value of ζ during the ith impulse. Now, for an efficient control we know that

$$\left|\Delta h_i\right| = u_{max}\,\Delta t_i \tag{10.12}$$

where Δt_i is the time duration of the ith firing. Since the Δh_i quantities move in a straight line for class 1 or class 3 initial conditions, we have

$$\left|\sum_{i=1}^{n} \Delta h_i\right| = \sum_{i=1}^{n} \left|\Delta h_i\right| \tag{10.13}$$

Using equations (10.11) through (10.13), equation (10.10) can be written as

$$-\sum_{i=1}^{n} \cos(\zeta_i - \delta_1)\Delta t_i = \delta_0 \sum_{i=1}^{n} \Delta t_i . \tag{10.14}$$

We notice from the form of the switching function discussed in chapter VIII that the firings repeatedly occur over a portion of the period $2\pi/r$ which is the period of the nutation circle. This suggests that there is a firing sector centered about the angular momentum line (as shown by $\pm\kappa$ in fig. 10.13) for which equation (10.14) becomes

$$-\sum_{i=1}^{m} \cos(\zeta_i - \delta_1)\Delta t_i = \sigma_0 \sum_{i=1}^{m} \Delta t_i . \tag{10.15}$$

where m is the total number of firings per nutation cycle. Obviously, if equation (10.15) is satisfied each nutation cycle then equation (10.14) will be satisfied.

In the nutation cycle firing sector the value of ζ_i changes between successive firings by an amount $2\pi r$, where 2π is the time for one spin revolution and r is the nutational rate. If we then multiply equation (10.15) by $2\pi r$ and make the assumption that the Δt_i values can be replaced by an average constant value then we obtain

$$-\sum_{i=1}^{m} \cos(\zeta_i - \delta_1)2\pi r = \sigma_0 \sum_{i=1}^{m} 2\pi r.$$

Now as $r \to 0$, we can use the mean value theorem in reverse to obtain

$$-\sum_{i=1}^{m} \int_{\zeta_i - \pi r}^{\zeta_i + \pi r} \cos(\zeta - \delta_1)d\zeta = \sigma_0 \sum_{i=1}^{m} \int_{\zeta_i - \pi r}^{\zeta_i + \pi r} d\zeta \qquad (10.16)$$

which is equivalent to

$$-2\int_{\delta_1 + \kappa}^{\delta_1 + \pi} \cos(\zeta - \delta_1)d\zeta = 2\sigma_0 \int_{\delta_1 + \kappa}^{\delta_1 + \pi} d\zeta \qquad (10.17)$$

where κ is the upper switching bound in the nutation circle shown in *figure 10.13. Integration of equation (10.17) then yields*

$$\sin \kappa = \sigma_0(\pi - \kappa). \qquad (10.18)$$

From our previous results, it was noted that as $\sigma_0 \to 0$ (class 3), we obtained continuous firings. Thus, $\kappa \to 0$ for σ_0 small

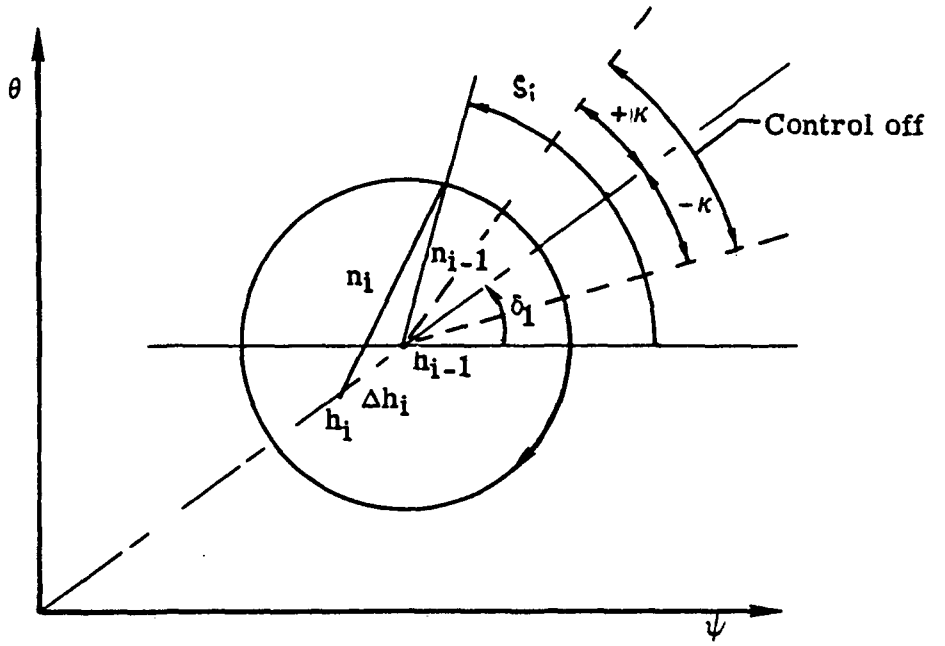

Figure 10.13.- Typical momentum and nutation shift due to an impulse for class 1 initial conditions.

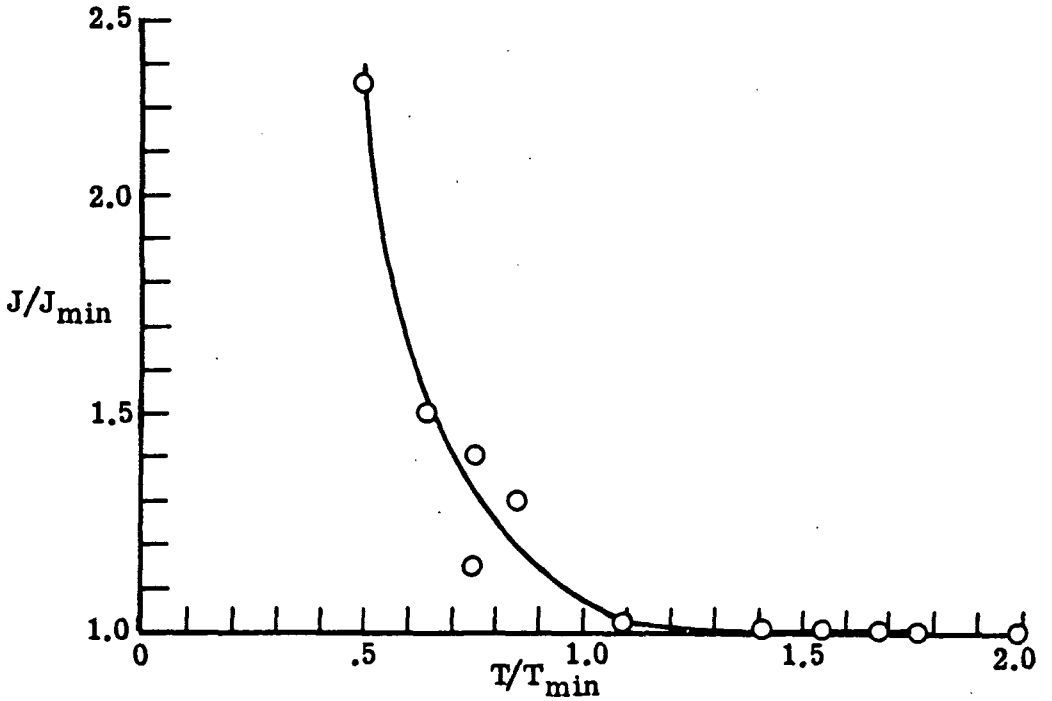

Figure 10.14.- Fuel consumption ratio as a function of the final time ratio.

and we can use the small angle approximations in equation (10.18) to obtain

$$\kappa = \frac{\sigma_0 \pi}{1 + \sigma_0} . \tag{10.19}$$

The total percentage of time that the jet cannot fire is then

$$\frac{\kappa}{\pi} = \frac{\sigma_0}{1 + \sigma_0} . \tag{10.20}$$

Thus, the total amount of time which the jets can fire is

$$\bar{T} = T\left[1 - \frac{\sigma_0}{1 + \sigma_0}\right]$$

$$= \frac{T}{1 + \sigma_0} . \tag{10.21}$$

The total number of firings which can occur in the time $\bar{T}$ is then

$$N = \frac{\bar{T}}{2\pi} \tag{10.22}$$

where 2π is the time for one spin revolution.

Finally, using equations (10.8), (10.21), and (10.22) in equation (10.9) gives

$$\frac{2\, u_{max} \pi}{9} \cdot \frac{T_{min}}{2\pi(1 + \sigma_0)} = J_{min}$$

or

$$T_{min} = \frac{9\, J_{min}(1 + \sigma_0)}{u_{max}} \tag{10.23}$$

where T_{min} is the approximate minimum time required to achieve J_{min}.

Recall from the discussion of the impulse optimal control that the minimum time was also proportional to the arc length of the nutation circle. In particular, for σ_0 small

$$T_{min} \approx \frac{\pi}{r}. \tag{10.24}$$

Since equation (10.23) does not depend on r, it was then assumed that the actual T_{min} was probably some weighted average of equations (10.23) and (10.24) and indeed the quantity

$$T_{min} = \frac{\dfrac{9\, J_{min}(1 + \sigma_0)}{u_{max}} + 2\pi\left(\dfrac{1}{r} + \dfrac{1}{2 - r}\right)}{2} \tag{10.25}$$

give a close approximation of the minimum final time necessary for $J \approx J_{min}$. The $1/(2 - r)$ term was added to produce the symmetry which was previously discussed.

A plot of J/J_{min} versus T/T_{min} is shown on figure 10.14 where J_{min} is given by equation (10.7) and T_{min} is given by equation (10.25). This curve has been checked for parameter variation in the following ranges and gives good agreement for a variety of combinations:

$$0 \leq \sigma_0 \leq 1$$

$$0 < r < 2$$

$$0 < u_{max} < 0.4.$$

It is seen that for $T/T_{min} > 1$, $J/J_{min} \approx 1$, and for $T/T_{min} < 1$ the fuel consumption increases rapidly until an absolute minimum time is reached. Equation (10.25) thus gives the control system designer a feel for the adjustments required to optimize the fuel consumption for a given final time.

XI. APPROXIMATE FEEDBACK OPTIMAL CONTROL

The optimal control solutions which have been developed so far provide only the open-loop control from a known set of initial conditions. If any errors arise in the system during a maneuver, they are not sensed and corrected, and can possibly drive the system unstable. The ultimate desire is to determine a relationship between the state variables and the adjoint variables so that an optimal closed-loop feedback control can be developed.

The determination of a general feedback relationship is a formidable, if not impossible, task. However, if we limit ourselves to class 1 and class 3 initial conditions, a final time greater than T_{min}, and small values of r, it is possible to develop a feedback logic which approximates the optimal control. Since we are primarily concerned with the theory of a feedback control and not the hardware, we shall assume that all the desired feedback quantities are measurable in some fashion.

A logical starting point in the development of our approximate theory is the switching function given by equation (8.25). In this function we have the four constants A_1, β_1, A_2, and β_2 (equivalent to the four unknown costate variables) that are related to the four state variables x_1 thru x_4 in some manner. By expanding on the ideas set forth in chapter X we shall obtain approximate feedback-relationships and thereby determine an approximate optimal control.

A. Simplification of Switching Function

By referring to tables 10.2 and 10.3, we notice that for class 1 (and class 3) solutions (cases 1 and 3) that $A_2/A_1 \ll 1$. Many solutions, in addition to the ones presented, have been studied and this trend always holds for σ_0 small and $T/T_{min} > 1$. Assuming these conditions to be true and that $r < 1$ equations (8.31) and (8.32) can be simplified to yield

$$D(t) \approx A_1 + A_2 \cos (rt + \beta_1 - \beta_2) \tag{11.1}$$

and

$$\delta(t) \approx rt + \beta_1 - \beta_2. \tag{11.2}$$

The switching function equation (8.30) then becomes

$$f_s = 1 - \left[A_1 + A_2 \cos (rt + \beta_1 - \beta_2)\right] \sin (t + \beta_1). \tag{11.3}$$

A plot of the switching function lower envelope given by equation (11.3) is shown in figure 11.1. It is seen that the length of the firing region is a function of $(A_1 - 1)$ and A_2 and that the phasing of the peak amplitude depends on $\beta_2 - \beta_1$.

B. Switching Function Phase Angles

The form of the switching function given by equation (11.3) gives an indication of the requirements for the phase angles. We notice that the frequency of the amplitude term, D(t), is the same as the nutation

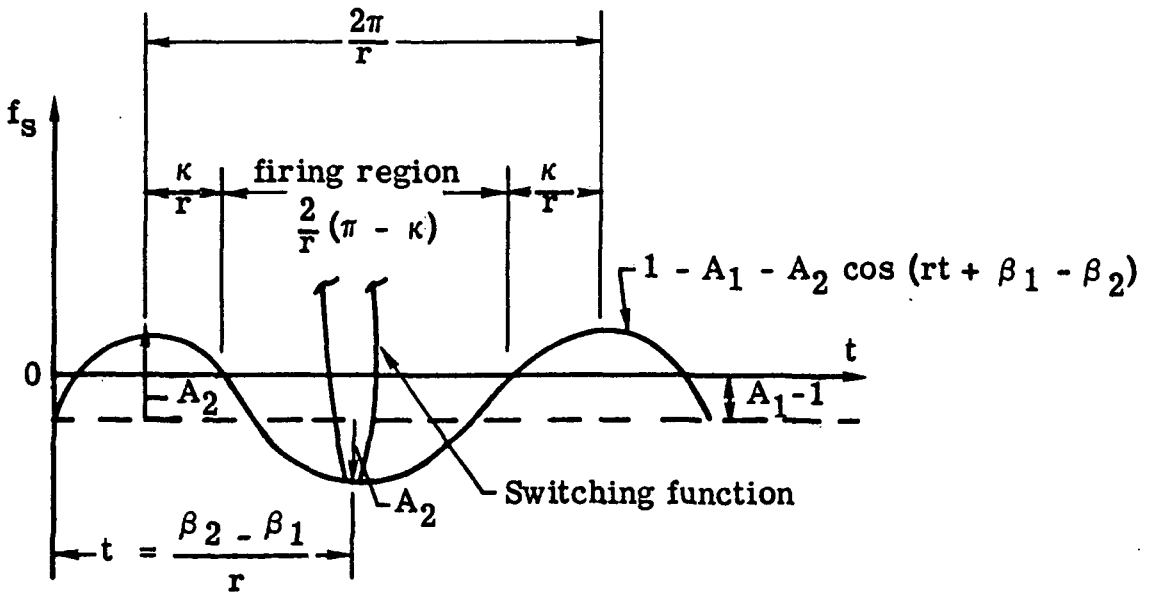

Figure 11.1.- Switching function lower envelope.

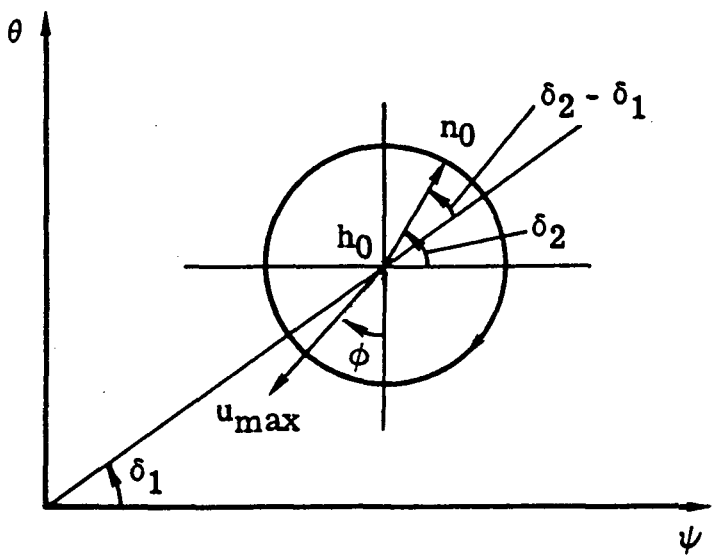

Figure 11.2.- Phase relationships in a typical ψ-θ trajectory.

frequency and that the sine function frequency is the same as the spin rate. To determine the physical significant of these terms, let us refer to figure 11.2. We see that the angles δ_1 and δ_2 are given by

$$\delta_1 = \tan^{-1}\left(\frac{x_{20}}{x_{10}}\right) \tag{11.4}$$

and

$$\delta_2 = \tan^{-1}\left(\frac{x_{40}}{x_{30}}\right).$$

Also, the roll angle φ denotes the orientation of the torque vector. In order to move the angular momentum in a straight line toward the origin, we see that the firing sector must be centered around the angle

$$\varphi = \frac{\pi}{2} - \delta_1. \tag{11.5}$$

This event should coincide with the time that the sine function of equation (11.3) is a maximum, i.e.

$$t + \beta_1 = \pi/2 \tag{11.6}$$

since this point is the center of the firing arc. By definition

$$\varphi = \Omega\tau = t$$

then the substitution of equation (11.5) into equation (11.6) gives

$$\beta_1 = \delta_1 = \tan^{-1}\left(\frac{x_{20}}{x_{10}}\right). \tag{11.7}$$

We further note from figure 11.2 that the initial nutation vector rotates to coincide with h_0 when

$$t = (\delta_2 - \delta_1 + \pi)/r. \tag{11.8}$$

In order to have the firing sector of the nutation circle centered around h_0, the cosine function in equation (11.3) must be a maximum at the time given by equation (11.8) or

$$(\delta_2 - \delta_1 + \pi) + \beta_1 - \beta_2 = 0. \tag{11.9}$$

Then using equation (11.7) we have

$$\beta_2 = \pi + \delta_2. \tag{11.10}$$

It can be seen from equation (11.4) that

$$\pi + \delta_2 = \tan^{-1}\left(\frac{-x_{40}}{-x_{30}}\right) \tag{11.11}$$

therefore,

$$\beta_2 = \tan^{-1}\left(\frac{-x_{40}}{-x_{30}}\right). \tag{11.12}$$

If we substitute the initial conditions for case 1 given by table 10.2 into equations (11.7) and (11.12), we obtain $\beta_1 = 0^\circ$ and $\beta_2 = -90^\circ$. By comparing these values with those of table 10.3 we see that the agreement is very good. A closed-form feedback relationship has, thus, been established to determine the switching function phase angles from the initial state variables. The problem is half solved;

it remains to also determine A_1 and A_2 as functions of the initial state variables.

C. Switching Function Amplitudes

The time duration of a thrust pulse is seen from figure 10.5(a) to be dependent upon the local amplitude of the switching function envelope. Since this envelope magnitude is continuously changing, the thrust durations are continuously changing. This fact (among others) makes a simple closed form relationship between the switching function amplitudes (A_1 and A_2) and the state vector (x) impossible to obtain. By making additional approximations, however, we can approach the exact solutions.

First, let us assume that during the thrusting and non-thrusting regions shown in figure 11.1 that the envelope has a constant amplitude. The switching function would then be similar to that shown in figure 11.3.

A switching function of this type appears to be nearly as efficient as the actual solution. The amplitude of the envelope during the non-thrusting regions is not important as long as it is less than one. To find the amplitude of the envelope during thrusting, we shall make use of the arguments developed in the preceding chapter.

From figure 11.1 we see that the non-firing region of the nutation circle can be expressed in terms of A_1 and A_2 as

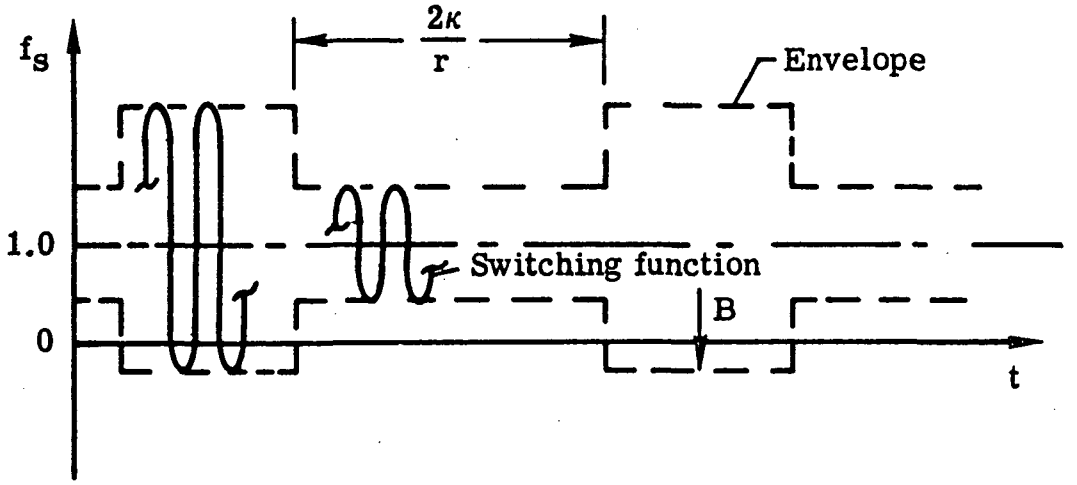

Figure 11.3.- Bi-level switching function.

$$A_2 \cos \kappa = A_1 - 1 \tag{11.13}$$

or

$$\lambda = \frac{A_2}{A_1 - 1} = \frac{1}{\cos \kappa} .$$

The substitution of equation (10.19) into equation (11.13) gives

$$\lambda = 1/\cos\left[\frac{\sigma_0(\pi - \delta_1)}{1 + \sigma_0}\right]. \tag{11.14}$$

We can obtain the equation for the lower envelope of the switching function equation (11.3) as

$$f_{s_E} = 1 - A_1 - A_2 \cos (rt + \beta_1 - \beta_2)$$

or (11.15)

$$f_{s_E} = - (A_1 - 1) \left[1 + \lambda \cos (rt + \beta_1 - \beta_2)\right] .$$

The bi-level switching function of figure 11.3 will have the same thrusting regions as the actual solution of equation (11.15) if we define the amplitude of equation (11.1) as follows

$$D(t) = B \text{ for } \left[1 + \lambda \cos (rt + \beta_1 - \beta_2) \right] > 0$$

or (11.16)

$$= .5 \text{ for} \left[1 + < \cos (rt + \beta_1 - \beta_2)\right] < 0$$

where B is a constant greater than one, which is yet to be determined, and λ is given by equation (11.14).

The duration of a firing pulse, Δt, can be seen from figure 11.3 to satisfy the equation

$$\Delta t = 2 \cos^{-1}\left(\frac{1}{B}\right). \tag{11.17}$$

Now using equations (11.17), (10.12), (10.21), and (10.22) in equation (10.9) in a manner similar to that of chapter X we obtain

$$2u_{max} \cos^{-1}\left(\frac{1}{B}\right) \frac{T}{(1 + \sigma_0)2\pi} = \left|h_0\right| \tag{11.18}$$

or

$$B = \frac{1}{\cos\left[\dfrac{\pi(1 + \sigma_0)\, h_0}{u_{max}\, T}\right]}$$

We now have all of the necessary ingredients to formulate an approximate optimal control.

D. Feedback Control Logic

Before proceeding further, let us summarize our present results. An approximate switching function has been derived of the form

$$f_s = 1 - D(t) \sin (t + \beta_1) \tag{11.19}$$

where $D(t)$ is determined from equations (11.16), (11.14), (11.7), (11.18), and (11.12). We note that equation (11.19) only depends upon the initial conditions and is therefore an approximation to the actual closed form solution. In fact, if we let $A_1 \approx B$, then A_2 can be determined equations (11.13) and (11.14). For case 1 of table 10.2 this approximation gives

$$A_1 \approx 1.021$$

$$A_2 \approx .042$$

which are very close to the exact values of table 10.3.

Because of the inaccuracies in the approximations as well as in the other aspects of the system, it is desirable to update our calculations as often as possible, i.e., to provide a feedback loop by which we can measure the control performance. Rather than a continuous feedback, however, it appears that a sample of the state vector once per nutation period would be sufficient. Referring to figure 10.13, we see that we could sample the state vector at the center of the control off sector and then compute the required switching function constants for the next nutation cycle. Any error which built up during one nutation cycle would then be removed during the next.

In summary, we have developed an approximate fuel-optimal control logic for a system for which the inertia ratio, r, is small, the final time is greater than T_{min}, and the initial conditions are of class 1

or class 3. The groundwork has also been laid for extending the approach to the more difficult class 2 and class 4 initial conditions.

XII. CONCLUSIONS

A comprehensive investigation has been made of the fuel-optimal control problem of reorienting a symmetrical spinning body by means of a single body-fixed jet within a prescribed time. From this investigation, we are led to the following conclusions:

(i) For an idealized mathematical model of a rigid symmetrical body, the state equations can be linearized, nondimensionalized, and transformed to a canonical form. The canonical state vector can be partitioned into uncoupled nutation and angular momentum vectors. This form is ideal for a physical interpretation of the spinning body motion and formulation of the optimal control problem.

(ii) For a single control jet of fixed size, the control torque, u, is bounded so that $0 \leq u \leq u_{max}$. Pontryagin's minimum principle for the bounded control yields a "bang-bang" optimal control. The switching function is periodic and cannot remain zero over a finite interval of time, therefore, a singular optimal control does not exist.

(iii) The evaluation of the optimal control reduces to solution of the two-point boundary value problem given by equations (8.13). These equations can only be solved numerically and, therefore, the synthesis of the optimal control is most difficult, if not impossible.

(iv) The optimal control, if it exists, is unique. Further, the lower bound on the minimum fuel consumption is

$$J(u) = \text{maximum of } \{|h_0|, |n_0|\}$$

and for a limited amount of fuel, only certain initial conditions can be controlled. An arbitrary initial state is controllable, if and only if, the condition of equation (8.18) are satisfied.

(v) An efficient computational algorithm and digital computer program is presented for solving the two-point boundary value problem for arbitrary initial conditions and system parameters. The approach of this paper offers several improvements over existing methods of solution. The computational algorithm as derived herein applies strictly to the subject problem. However, the method of derivation is completely general and similar results can be obtained for a wide variety of other linear optimal control problems.

(vi) The motion of the angular momentum vector obtained from actual solutions is similar to that of a two-impulse optimal control. That is, when the initial nutation circle excludes the origin, the angular momentum tends to move in a straight line. Otherwise, it doesn't.

(vii) For the same initial conditions, the switching function (or control) is the same for an inertia ratio of r (where $r < 1$) as it is for an inertia ratio of $(2 - r)$. This fact may possibly be utilized in the synthesis of the difficult problem which results when $r > 1$.

(viii) For a final time (T) greater than the value given by equation (10.25), the minimum fuel consumption is very near to the lower bound. This equation gives the control system designer a

feel for the system parameter adjustments required to optimize fuel consumption for a given final time. For example, a value of $r = .5$ produces a higher fuel consumption than a value near zero or near two.

(ix) The switching function for classes 1 and 3 initial conditions with $r < 1$ can be closely approximated by equation (11.3). A similar equation can be derived for classes 2 and 4 initial conditions (where $A_1/A_2 \ll 1$), and for $r > 1$ we can further derive an additional set of equations. The basic logic that must be employed in an approximate optimal control is derived from the simplified switching function for σ_0 and r small.

(x) The results of this paper lay the groundwork for a more extensive study of fuel-optimal control for spinning bodies and possibly for the solution to the difficult non-linear problem.

XIII. APPENDICES

A. Modified Jordan Transformation Matrix

1. Jordan Canonical Form - It can be shown that it is always possible to find a nonsingular matrix, P, that will transform an arbitrary square matrix, A, into the Jordan canonical form through the similarity transformation

$$\Lambda = P^{-1}AP . \tag{A-1}$$

The Jordan canonical matrix Λ is a quasi-diagonal matrix of the form

$$\Lambda = \begin{bmatrix} \Lambda_1 & & & \\ & \Lambda_2 & & \\ & & \ddots & \\ & & & \Lambda_p \end{bmatrix} \tag{A-2}$$

where p is the number of distinct eigenvalues of A and each Jordan block, Λ_i, has the form

$$\Lambda_i = \begin{bmatrix} \lambda_i & 1 & & \\ & \lambda_i & 1 & \\ & & \ddots & \ddots \\ & & & 1 \\ & & & \lambda_i \end{bmatrix}, \qquad i = 1,2, \ldots p. \tag{A-3}$$

The order of each Λ_i block is the multiplicity of the corresponding distinct eigenvalue, λ_i, of A.

2. Modified Jordan Canonical Form - In generating the Jordan matrix of (A-2), the complex-conjugate eigenvalues are treated in exactly the same way as real eigenvalues. It is convenient, however, to transform the Jordan matrix into a modified form which has only real elements. This modification is based on the fact that one pair of complex conjugate vectors contains all the essential information of the pair.

Let us consider a Jordan canonical matrix with a pair of complex conjugate eigenvalues on the diagonal. This matrix has the form

$$\Lambda = \begin{bmatrix} \Lambda_1 & & & & \\ & \ddots & & & \\ & & a+ib & 0 & \\ & & 0 & a-ib & \\ & & & & \ddots \\ & & & & & \Lambda_p \end{bmatrix} \qquad \text{(A-4)}$$

where the complex eigenvalues are $\lambda = a \pm ib$. The Jordan matrix λ can be transformed to the modified Jordan form

$$\bar{\Lambda} = \begin{bmatrix} \Lambda_1 & & & & \\ & \ddots & & & \\ & & a & b & \\ & & -b & a & \\ & & & & \ddots \\ & & & & & \Lambda_p \end{bmatrix} \qquad \text{(A-5)}$$

by the similarity transformation

$$\bar{\Lambda} = K^{-1} \Lambda K \tag{A-6}$$

where

$$K = \begin{bmatrix} 1 & & & & \\ & \ddots & & & \\ & & \begin{bmatrix} 1/2 & -i/2 \\ 1/2 & i/2 \end{bmatrix} & & \\ & & & \ddots & \\ & & & & 1 \end{bmatrix} \tag{A-7}$$

and the full 2×2 block occupies the place taken by the complex conjugate pair in (A-4).

The substitution of (A-1) into (A-6) gives

$$\bar{\Lambda} = P^{-1} A \bar{P} \tag{A-8}$$

where

$$\bar{P} = PK \tag{A-9}$$

is the modified Jordan transformation matrix. Not only does $\bar{\Lambda}$ have all real elements but, more significantly, P also has only real elements. The transformation for the modified Jordan form, (A-8), is then of the same form as that of the Jordan normal form given by (A-1).

B. Physical Significance of Canonical Variables

In this section a physical significance is attached to both the canonical state and control variables. The understanding of this relationship is of the utmost importance in understanding and interpreting the optimal control solutions.

1. Canonical State Variable - It is well known from the classical theory of rigid body dynamics that in the absence of external torques, a body spinning about an axis of symmetry cones about the angular momentum vector ($\vec{H}$), which is fixed in space. We also know that the nutation cone semi-angle remains constant and its magnitude can be shown to be $\left[(\dot{\psi}/r)^2 + (\dot{\theta}/r)^2\right]^{1/2}$ for θ small. Let ψ_h and θ_h denote the Euler angle orientations of the x_h, y_h, z_h coordinate system relative to the inertial system X_I, Y_I, Z_I with x_h along $\vec{H}$ as shown in figure B.1. Also, let ψ_n and θ_n denote the Euler angle orientation of the nonspinning body axis system relative to the x_h, y_h, z_h system as shown in figure B.2.

Obviously, the maximum values of ψ_n and θ_n are the magnitude of the cone semi-angle, i.e

$$\left|\theta_n\right|_{max} = \left|\psi_n\right|_{max} = \left[\left(\frac{\dot{\psi}}{r}\right)^2 + \left(\frac{\dot{\theta}}{r}\right)^2\right]^{1/2}. \qquad \text{(B-1)}$$

In keeping with the linearizing assumptions that θ and $\dot{\psi}$ are small it is seen that θ_n, ψ_n and $\dot{\theta}$, as well as θ_h must also be small.

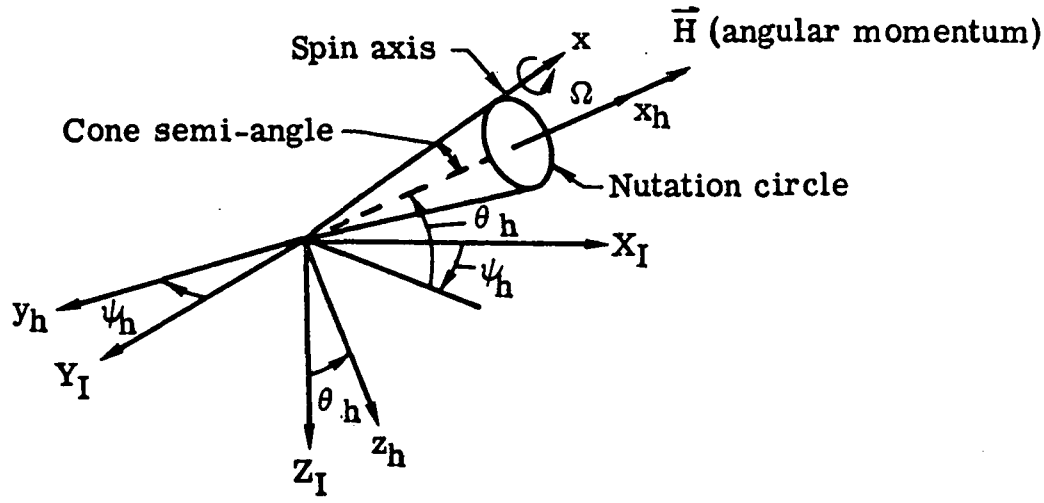

Figure B.1.- Angular momentum coordinates (ψ_h, θ_h).

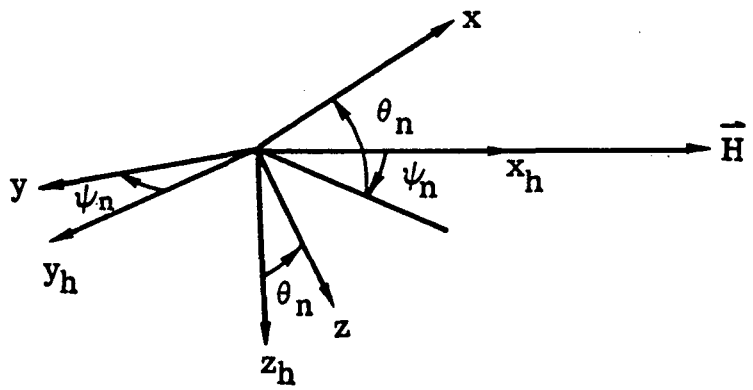

Figure B.2.- Nutation coordinates (ψ_n, θ_n).

It can then be shown that

$$\theta \approx \theta_h + \theta_n \tag{B-2}$$

and

$$\psi \approx \psi_h + \psi_n.$$

That is, the total angular displacements in the ψ-θ plane is the vector sum of the angular displacements of the angular momentum vector and the nutation vector as shown in figure B.3.

Using equation (7.4) and the definition of the angular momentum components along the x, y, z axes we have

$$\begin{aligned} H_x &= I_a(\omega_x + \Omega) = I_a\Omega, \\ H_y &= I_t\omega_y = I_t \frac{d\theta}{d\tau}, \end{aligned} \tag{B-3}$$

and

$$H_z = I_t\omega_z = I_t \frac{d\psi}{d\tau}.$$

We can also write these components as the orthogonal projection of $\vec{H}$ on the body axes, i.e.

$$\begin{aligned} H_x &= |\vec{H}| \cos \psi_n \cos \theta_n, \\ H_y &= -|\vec{H}| \sin \psi_n, \end{aligned} \tag{B-4}$$

and

$$H_z = |\vec{H}| \cos \psi_n \sin \theta_n.$$

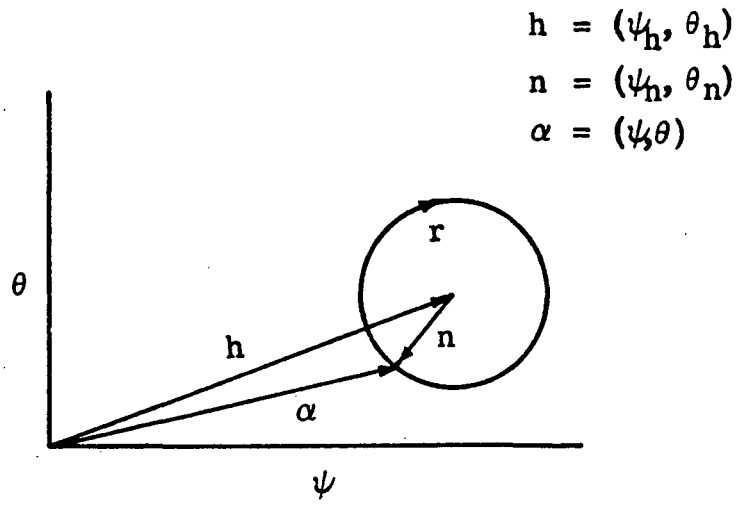

Figure B.3.- Torque-free nutational motion in ψ-θ plane.

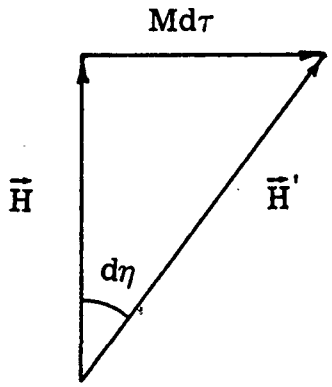

Figure B.4.- Deviation in angular momentum due to an impulsive torque.

Since ψ_n and θ_n are small, we obtain from equations (B-4)

$$\psi_n \approx - H_y/H_x$$

and (B-5)

$$\theta_n \approx H_z/H_x.$$

The substitution of equations (B-3) into equations (B-5) then leads to

$$\psi_n = - \dot{\theta}/r$$

and (B-6)

$$\theta_n = \dot{\psi}/r.$$

Using equations (B-6) we also see from equations(B-2) that

$$\psi_h = \psi + \dot{\theta}/r$$

and

$$\theta_h = \theta - \dot{\psi}/r. \qquad \text{(B-7)}$$

Let us now seek to find the vector x in terms of the Euler angles and their derivatives. The premultiplication of equation (7.19) by $\bar{P}^{-1}$ gives the canonical state vector x in terms of the original state vector y as

$$x = \bar{P}^{-1} y. \qquad \text{(B-8)}$$

Then from equations (7.14), (7.20), and (B-8) we obtain the following expressions for the canonical state variables in terms of the non-dimensional Euler angle quantities:

$$x_1 = \psi + \dot{\theta}/r,$$

$$x_2 = \theta - \dot{\psi}/r,$$

$$x_3 = -\dot{\theta}/r, \tag{B-9}$$

and

$$x_4 = \dot{\psi}/r.$$

Comparing equations (B-9) with equations (B-6) and (B-7) we have

$$x_1 = \psi_h,$$

$$x_2 = \theta_h,$$

$$x_3 = \psi_n, \tag{B-10}$$

and

$$x_4 = \theta_n.$$

Thus, in the ψ-θ plane, x_1 and x_2 are components of the angular momentum vector (h) and, x_3 and x_4 are components of the nutation vector (n).

The above conclusion can also be deduced from the following solutions to equations (7-10) with $\nu = 0$

$$\theta = \theta_0 - \frac{\dot{\psi}_0}{r} + \frac{\dot{\theta}_0}{r} \sin rt + \frac{\dot{\psi}_0}{r} \cos rt,$$

$$\psi = \psi_0 + \frac{\dot{\theta}_0}{r} + \frac{\dot{\psi}_0}{r} \sin rt - \frac{\dot{\theta}_0}{r} \cos rt. \tag{B-11}$$

Rearranging, squaring, and adding equations (B-11) yields:

$$\left[\theta - (\theta_0 - \dot{\psi}_0/r)\right]^2 + \left[\psi - (\psi_0 + \dot{\theta}_0/r\right]^2 = \left(\frac{\dot{\theta}_0}{r}\right)^2 + \left(\frac{\dot{\psi}_0}{r}\right)^2 \qquad \text{(B-12)}$$

which is the equation for a circle in the ψ-θ plane as shown in figure B.3 with the center at $h_0 = (x_{1_0},\ x_{2_0})$ and a radius of $|n_0| = \sqrt{x_{30}^2 + x_{40}^2}$. It can further be shown from the derivative of equations (B-11) that the nutation arm rotates about the angular momentum arm at the nondimensional rate r.

2. Canonical Control Variable - For an interpretation of the nondimensional control variable u, let us refer to figure B.4. If the vehicle is undergoing pure spin about the spin axis the angular momentum is $\left|\vec{H}\right| = I_a\Omega$. When the jet is fired, an impulsive torque $M\,d\tau$ is applied to the system in the time $d\tau$. The resulting incremental change, $d\eta$, in the orientation of $\vec{H}$ to $\vec{H}'$ is given as

$$d\eta = \frac{M\,d\tau}{I_a\Omega}. \qquad \text{(B.13)}$$

By dividing equation (B-13) by the quantity $\Omega\,d\tau$ we have from equations (7.7) and (7.24)

$$\dot{\eta} = \frac{M}{I_a\Omega^2} = u.$$

Thus, the canonical control variable u is the nondimensional precession rate (radians per radian of spin) of the angular momentum vector $\vec{H}$.

XIV. REFERENCES

1. Garner, H. D.; and Reid, H. J. E., Jr.: Simulator Studies of Simple Attitude Control For Spin-Stabilized Vehicles. NASA TN D-1395, September 1962.

2. Grubin, C.: Generalized Two-Impulse Scheme for Reorienting a Spin Stabilized Vehicle. Progress in Astronautics and Rocketry. Vol. 8, Academic Press Inc., 1962, pp. 649-668.

3. Windeknecht, T. G.: A Simple System for Sun Orientation of a Spinning Satellite. (Preprint) 61-204-1898, paper presented at the National IAS and ARS Joint Meeting (Los Angeles, Calif.), June 1961.

4. Rasmussen, R. O.; Lanzaro, A.; Sinott, N. F.; and Schafer, D. R.: Attitude Control for Spinning Sounding Rockets. Paper presented at AIAA Sounding Rocket Vehicle Technology Specialist Conference (Williamsburg, Va.), Feb. 27-Mar. 1, 1967.

5. LeCompte, G. W.; and Bland, J. G.: Simply Mechanized Attitude Control for Spinning Vehicles. J. Spacecraft, Nov.-Dec. 1964.

6. Freed, L. E.: Attitude Control System for a Spinning Body. (Preprint) 61-207-1901, paper presented at the National IAS and ARS Joint Meeting (Los Angeles, Calif.), June 1961.

7. Adams, J. J.: Study of an Active Control System for a Spinning Body. NASA TN D-905, June 1961.

8. Lange, Benjamin; Fleming, Alan W.; and Parkinson, Bradford,W.: Control Synthesis for Spinning Aerospace Vehicles. J. Spacecraft, Vol. 4, No. 2, Feb. 1967, pp. 142-156.

9. Yin, M.; and Grimmell, W. C.: Optimal and Near-Optimal Regulations of Spacecraft Spin Axes. IEEE Transactions on Automatic Control, Vol. AC-13, No. 1, Feb. 1968, pp. 57-64.

10. Windeknecht, T. G.: Optimal Stabilization of Rigid Body Attitude. J. Math, Analysis and Applications, Vol. 6, 1963, pp. 325-335.

11. Lieberman, S. I.; and Margosian, Z.: A Class of Time-Optimal Velocity Control Laws for a Spinning Space Vehicle. IEEE Transactions on Automatic Control, Vol. AC-9, No. 1, Jan. 1964, pp. 286-287.

12. Athans, Michael; Falb, Peter; and Lacoss, Richard T.: Time-Optimal Velocity Control of a Spinning Space Body, IEEE Transactions on Applications and Industry, Vol. 82, July 1963, pp. 206-213.

13. De Does, Dirk H.: Time Optimal Attitude Control of a Spinning Vehicle. American Astronautical Society Science and Technology Series, Vol. 11, 1967, pp. 301-317.

14. Greenwood, D. T.: Principles of Dynamics. Prentice-Hall, Inc., Englewood Cliffs, N. J., 1965, p. 418.

15. Ogata, K.: State Space Analysis of Control Systems. Prentice-Hall Inc., Englewood Cliffs, N.J., 1967, pp. 141-143.

16. Pontryagin, L. S., et al.: The Mathematical Theory of Optimal Processes. J. Wiley and Sons, N. Y., 1962.

17. Athans, M.; and Falb, P. L.: Optimal Control. McGraw-Hill Book Co., N.Y., 1966, p. 299.

18, MacIntyre, J. E.: Guidance, Flight Mechanics and Trajectory Optimization, Vol. 13 - Numerical Optimization Methods. NASA CR-1012, 1968.

19. Neustadt, L. W.; and Paiewonsky, B. H.: On Synthesizing Optimal Controls. Automatic and Remote Controls, Proceedings of the Second Congress of the International Federation of Automatic Control, Butterworths, London, 1964, pp. 283-291.

20. Fletcher, R.; and Powell, M. D. D.: A Rapidly Convergent Descent Method for Minimization. Computer J., Vol. 6, No. 2, July 1963, pp. 163-168.

21. Davidson, W. C.: Variable Metric Method for Minimization. A. E. C. Research and Development Report, ANL-599((Rev.), 1959.

22. Poricelli, Giacomo; and Connolly, Albert: Optimal Attitude Control of a Spinning Space-Body--A Graphical Approach. IEEE Transactions on Automatic Controls, Vol. AC-12, No. 3, June 1967, pp. 241-249.

XV. VITA

The author was born at [redacted], on [redacted]

He received his elementary education in Avon Park, Florida, and in Auburn, Alabama, and graduated from Auburn High School in June 1954. He entered Auburn University in September 1954 and received a Bachelor of Mechanical Engineering (with honor) in August 1958. He was a member of the R.O.T.C. and also received a commission in the U.S. Army Signal Corps. As an undergraduate he was elected to membership in the Pi Mu Epsilon, Pi Tau Sigma, Tau Beta Pi, and Phi Kappa Phi Honorary Societies. In September 1958, while waiting to enter the service, he accepted a position as an analytical design engineer with Pratt and Whitney Aircraft, West Palm Beach, Florida. He then served a 6-month tour in the U.S. Army from May 1959 to September 1959. Upon release from the service, he accepted a position as an aerospace engineer with the NASA, Langley Research Center. Under the NASA graduate program, he attended the University of Virginia the fall semester of 1960 and was awarded the degree of Master of Applied Mechanics in August 1964. During the 1965-1966 academic year he was in residency at Virginia Polytechnic Institute to pursue further graduate work toward a Doctor of Philosophy degree. He is presently employed as Head of the Flight Dynamics Section of the Flight Vehicles and Systems Division of the NASA, Langley Research Center. He is married, has two children and resides in Hampton, Virginia.

Robert T. Kingate